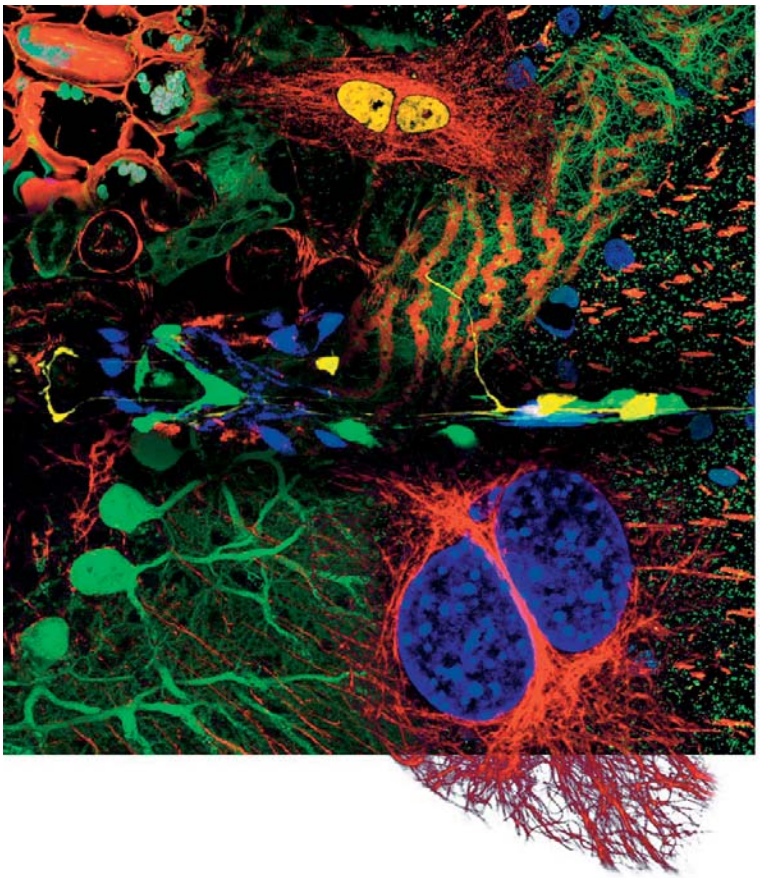

Confocal Microscopy

Alberto Diaspro • Mario Faretta • Paolo Sapuppo

Leica
MICROSYSTEMS

Confocal Book

Alberto Diaspro
LAMBS-MicroScoBio,
Department of Physics, University of Genoa, Genoa,
Italy Istituto FIRC di Oncologia Molecolare
FIRC Institute of Molecular Oncology, Milan, Italy
diaspro@fisica.unige.it
URL: http://www.lambs.it

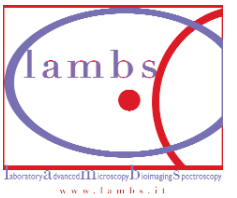

Mario Faretta
European Institute of Oncology
Imaging Centre, IFOM-IEO Campus for Oncogenomics, Milan, Italy
mario.faretta@ifom-ieo-campus.it
URL: http://www.ifom-ieo-campus.it (click on the facilities submenu)

The IFOM-IEO campus

Paolo Sapuppo
Leica Microsystems SPA, Milan, Italy
paolo.sapuppo@leica-microsystems.com
URL: http://www.confocal-microscopy.com

Content

“We have both seen many things but we still want to see more…”

Mercanti di Liquore

Microscopy and biology: in 1665 Robert Hooke observed the cellular structure in a piece of cork with the microscope he designed. The organisation of these structures reminded him of "cells" in a monastery. This analogy led to the name "cell" for the fundamental units of life. The photo (by A. Diaspro) shows the cell of St. Francis in the monastery of Cortona (17th century).

Introduction

In 1665 Robert Hooke was experimenting with his newly designed instrument that today we know as optical microscope. When observing the structure of a cork section, he noticed the orderly arrangement of little boxes which reminded him of the cells in monasteries where monks usually spent their lives (see picture, p. 4). Following this idea, he realised that the best term to describe such structures would be "cells". The name of the basic elements of life is therefore a reminder of the close relationship between life sciences and microscopy; a liaison that further evolved and strengthened in the following centuries.

On the wave of the scientific and technological revolution in the 20th century, microscopy underwent profound transformations. New tools were developed to reach the theoretical resolution limits that were derived from physical laws of the behaviour of light in nature. Some tools even allowed these limits to be overcome. As a result, we gained information from the living world at a resolution of 200 nm and better – a performance that scientists in the first half of the 19th century would not have even thought of. Among these instruments, the laser scanning confocal microscope provided an incredible breakthrough in our understanding of living systems by introducing the 3rd spatial dimension into the landscape of the biological world.

A dramatic mutation consequently took place – transforming optical microscopy from a mere tool for scientific investigations into a new autonomous research field. Here, extremely different competences were brought together: physics, biology, engineering, chemistry and information technology. The evolution in fluorescence microscopy requires a completely new approach to this technology – even for those who just apply it as a tool. Using the microscope as a "black box" without knowing the basic principles of how it works leaves a significant part of its capabilities unused. The aim of this booklet is to provide a short summary of basic concepts – and to make the reader interested in consulting more detailed literature on the subject.

The first part focuses on a brief description of laser scanning confocal microscopy. It begins with an introduction of basic optical concepts in image formation. Then, an overview of the features of a confocal microscope is given. Advantages and disadvantages are discussed in comparison with a conventional widefield fluorescence microscope. Inserts provide more details on specific technical aspects. As already mentioned, a detailed description of the optical theory of the microscope is far beyond the scope of this booklet. Nevertheless, the authors aim to encourage discussion of important topics that are frequently ignored when experiments with fluorescence microscopes are planned.

From the description of a confocal microscope, the discussion moves to an overview of live-cell and spectral imaging – two developments that have gained extremely high importance in the biomedical research field. The first part ends with an introduction to *Fluorescence Recovery After Photobleaching* (FRAP) and *Förster Resonance Energy Transfer* (FRET). These new tools in the study of molecular dynamics and interactions are assuming a key role in the solution of the structure-function paradigm in the post-genomic era.

The second part of the book is devoted to the latest revolution in optical microscopy: the two photon microscope. A brief introduction on the physics ruling two photon-excitation is presented for a reader appreciation of the advantages and limitations of the so-called "nonlinear microscope". The setup of a two-photon system is then introduced as a supplementary subject to confocal laser scanning microscopes. The book closes with an overview of two-photon microscopy applications in the biomedical research field.

A list of essential literature on the subject is also provided.

1

1. Fluorescence Laser Scanning Confocal Microscopy (LSCM): from Euclid to Superstrings

Nowadays, fluorescence microscopy is an important and fundamental tool for biomedical research. Optical microscopy is almost non-invasive and allows highly spatially resolved images of organisms, cells, macromolecular complexes and biomolecules to be obtained. Generally speaking, the architecture of the observed structures is not significantly modified and the environmental conditions can be kept very close to physiological reality. Correct conditions are a prerequisite for an analysis of structure-function relationships and allow excellent reproduction of the biological network that regulates life. The maximum resolution in conventional optical microscopy is around 200 nm (figure **1**).

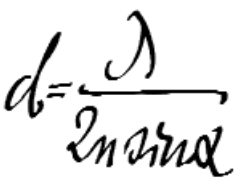

Figure **1**: The formula of Ernst Abbe (1840-1905), describing the resolution limit of conventional optical microscopes. The capability to distinguish two objects as separate entities depends on the wavelength of the collected light (λ), on the angular aperture of the objective lens ($\sin\alpha$) and the refractive index (n), a parameter describing the property of light propagation when the lens is immersed in a medium.

This allows efficient analysis of subcellular structures. Recently invented technologies, e.g. structured illumination, 4PI and STED, provide significantly higher resolution. Electron microscopy features a much higher resolving power which is about two orders of magnitude better than conventional optical microscopy. Unfortunately, it requires a sample preparation that is entirely incompatible with life. Although fluorescence microscopy cannot resolve the structure of single macromolecules, it can accomplish functional analysis. Fluorescence measurements are for example often used to characterise kinetic rates in biochemical reactions, thereby jumping towards nanoscopic analysis, which is the investigation of parameters of the world at single-molecule level (figure **2**, p.8).

The development of fluorescence microscopy was revolutionised with the invention of Laser Scanning Confocal Microscopy (LSCM). With its unique three-dimensional representation and analysis capabilities, this technology gives us a more real view of the world. Further technological improvements increased the number of dimensions in microscopic imaging. First, a fourth dimension was added by repeatedly measuring three-dimensional data in time (4D microscopy, xyzt). A second step was the introduction of spectral analysis of the emitted light (5D microscopy, xyztλ). Further complexity was introduced by combining these techniques with the latest technologies, particularly fluorescence lifetime imaging (FLIM), leading to six- and more-dimensional data. The present chapter introduces some basic optical concepts which are followed by an overview of microscopy evolution. Here, fluorescence widefield and confocal microscopy are compared. In conclusion, the chapter gives a brief idea of how their features allow virtual navigation in the above mentioned six dimensions.

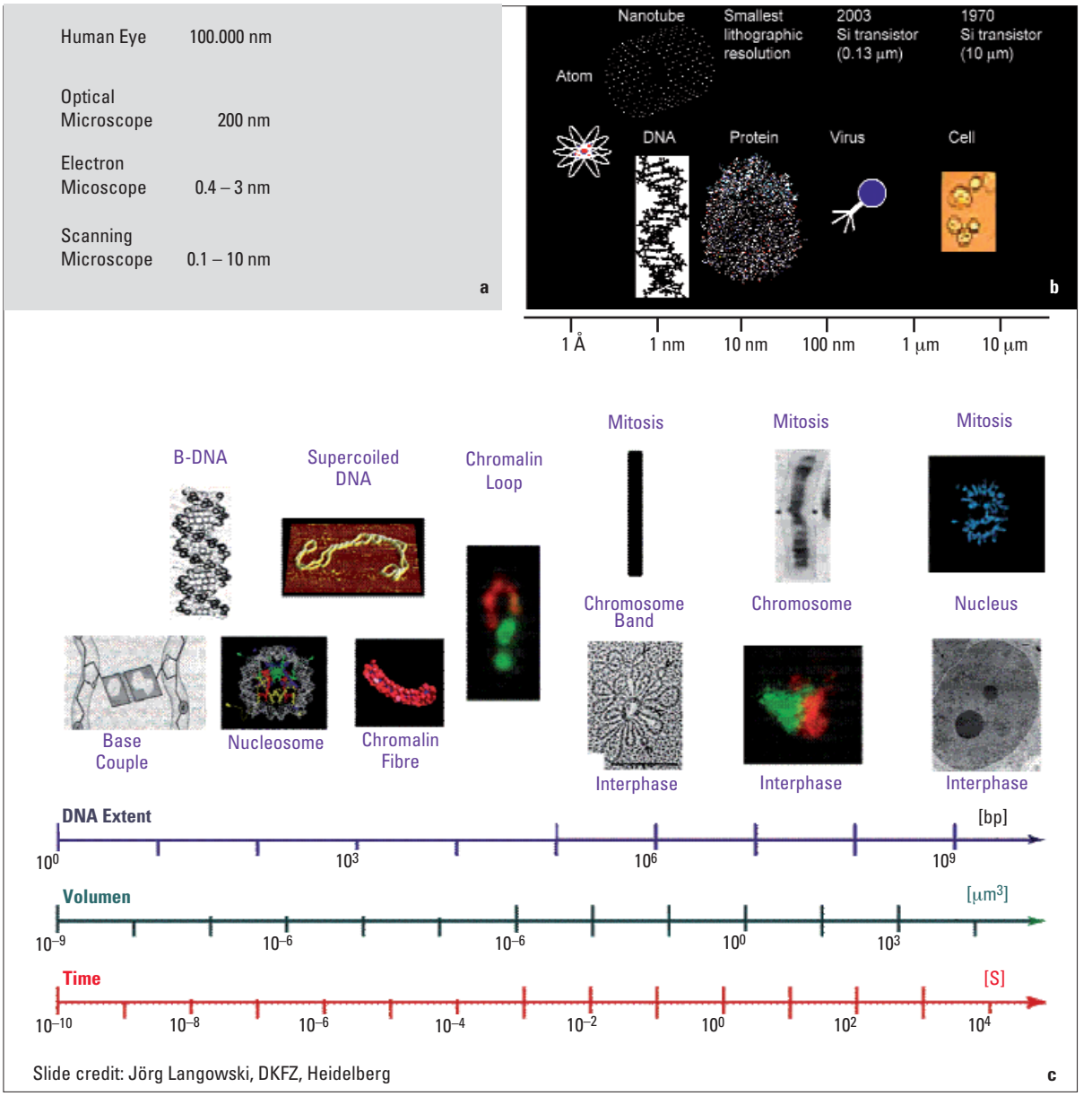

Figure **2**: Dimensional scale of nature in relation to the resolution capacity of available instruments. Figure 1a: Resolution limits of optical and electron microscopes. Figure 1b: Scale of the linear dimension of fundamental components of living material. Figure 1c: Volumetric and temporal scale in relation to the extension of cellular genetic material.

1.1 Image Formation in Fluorescence Microscopy: Point Spread Functions, Resolving Power, Contrast and Sampling Rate

The nature of the fluorescence process requires some key elements in optical systems. To excite fluorescence, obviously an illumination source must be delivered onto the sample. Illumination is accomplished by a series of lenses which usually consist of a collimator and an objective. The detection of the emitted signal then requires an optical element for light collection (the objective lens) and a detector (the human eye, a CCD camera or a Photomultiplier Tube (PMT). The geometrical arrangement of the above mentioned elements makes the difference between widefield and confocal systems. This classification will be discussed in the following chapter. The performance and limitations of each system depend on a common key element: the objective lens. As in all optical systems, diffraction limits the capabilities of the system. The objective lens can only collect photons within a fixed solid angle that is determined by the Numerical Aperture (NA). The NA is the product of the refractive index (n) of the immersion medium and the sine of the angular aperture of the lens (sinα), see figure **3a**. On the other hand, fluorescence is emitted isotropically in all spatial directions.

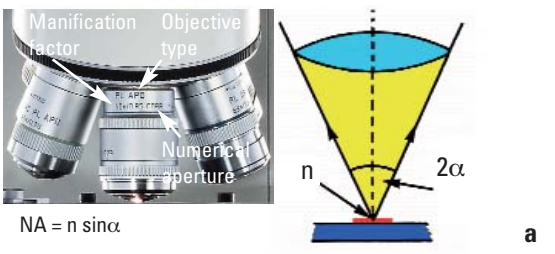

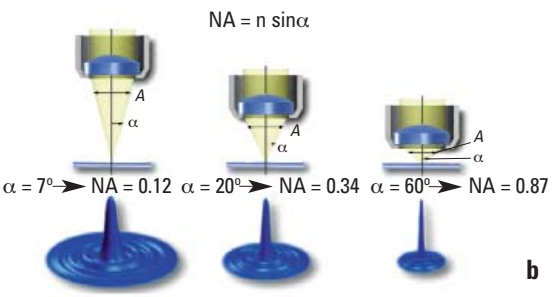

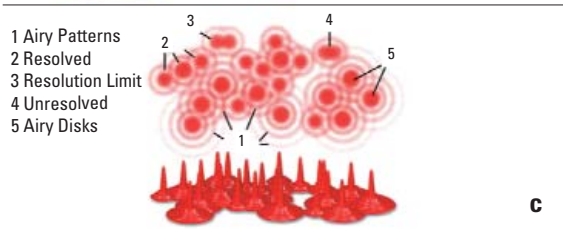

As the collected emission is only part of all emitted light, information is lost. Higher spatial frequencies do not pass through the aperture. As a consequence, the resolving power is limited, i.e. details below the resolving power cannot be separated. In diffraction-limited optical systems, a point-shaped object is reproduced as an Airy pattern, a disc surrounded by concentric rings. The disc's diameter (and the ring pattern) is defined by the objective's NA and the wavelength of the light. As long as the object's dimensions are smaller than the resolving power, the image of these structures (e.g. a single molecule or an organelle like a mitochondrion) will always be represented as Airy patterns (figure **3b**) with 180 – 200 nm in the best case. The spatial distribution of light in the three dimensions when emitted from a point is called the *Point Spread Function* (PSF). This function provides a measure of the microscope's performance. The intensity distribution of a complex structure (above the resolution limit) can be represented by superposition (convolution) of a series of single point objects. The image is then constructed as the superposition of the point spread functions of these point objects (figure **3c**). The ability to discriminate two objects as separate entities is referred to as the microscope's resolving power. The Rayleigh criterion (see insert 1) defines two objects as resolved if the distance is sufficiently large to separate the corresponding PSFs at least by one minimum (dark fringe between disc and first ring). The PSF of a microscope can be identified by imaging point-like objects, e.g. fluorescence beads of less than 200 nm in diameter, and then measuring the parameters of the diffraction pattern. This method also reveals optical aberrations that may compromise the system's performance.

Figures **3 a,b,c**: Numerical aperture, resolution and point spread function. Figure **3a**: Parameters which define an objective lens: Type (optical correction), magnification and numerical aperture (the formula for numerical aperture is given as: NA = n sinα, these parameters are shown in the figure). Figure **3b**: Numerical aperture and point spread function. The images of the objects are limited by the resolution which is given by the Abbe formula and coincides with the Airy distribution. Figure **3c**: The image is formed by superposition of the contributions of the single PSFs, which are generated by diffraction at the object.

The definition of resolving power also requires consideration of a second parameter controlling the *visibility*: the contrast. If the signal-to-noise ratio is too low, it will be very difficult to find the values for the theoretical resolution limit. The above mentioned definition of resolving power therefore depends on the quality of the collected images.

When evaluating the performance of an optical microscope, one has to remember that all considerations made so far assume continuous light intensity distributions. In reality, data collection by detectors (the human eye or a digital detector) in widefield or confocal microscopes is a result of a sampling operation at a defined frequency. The discrete values of intensity are given as bit-depth: monochromatic image bit-

Insert 1: **Resolution and PSF**

The resolution in an optical microscope is limited by the diffraction of light. Objects that are smaller than the diffraction limit will produce intensity distributions as shown in box **1**, figures **a** and **c**, p. 11. These patterns are named point spread functions. In xy, the pattern, which is called *Airy distribution*, features a central point surrounded by concentric rings. The profiles in xy and xz planes are shown in figures **b** and **d**. The elongated shape in the direction of the optical axis demonstrates the system's anisotropy. The image formation is ruled by the global PSF_{tot}, i.e. the product of the illumination and detection PSFs:

$$PSF_{tot}(x,y,z) = PSF_{ill}(x,y,z) \cdot PSF_{de}(x,y,z)$$

The lateral and axial extensions of the PSF_{tot} provide a measurement of the system's spatial resolution through the Full Width at Half Maximum (FWHM):

(1) $$\frac{0{,}51 \cdot \lambda}{NA}$$

where NA is the numerical aperture of the objective lens. The value 1.22λ/NA is the diameter of the first dark ring and referred to as a unit of measurement for the spatial resolution named Airy Unit (AU). A similar consideration can be applied to the measurement of the axial resolution. The z-extension of the first dark ring (figures **1b** and **d**) is provided by:

(2) $$1{,}67 \cdot \frac{n \cdot \lambda}{NA^2}$$

where n is the refractive index of the immersion medium (air, oil or water). In widefield microscopy the illumination apparatus creates a homogenous intensity distribution through a volume extending over a considerable thickness outside the focal plane with an energy flux that is constant throughout the three dimensions ($PSF_{ill}(x,y,z)$ = const). Consequently, the system's resolution is determined by the detection PSF.

The wavelength λ is the wavelength of the emitted light. In confocal microscopy the scanned laser beam produces an image in the focal plane corresponding to an Airy distribution depending on the excitation wavelength. PSF_{de} is instead the projection of the pinhole into the focal plane. For image acquisition, the pinhole diameter is set to cover the projected laser beam diameter. As a consequence, formula 1 and 2 efficiently provide an estimate of the lateral and axial resolutions in a confocal microscope if λ is set to the excitation wavelength. The formula 2 is an approximation of the real FWHM provided by:

(2[1]) $$\frac{0{,}88 \cdot \lambda_{exc}}{(n - \sqrt{n^2 - NA^2})}$$

Another criterion employed to evaluate spatial resolution is the ability to distinguish two objects as separate entities according to their relative distance. This Rayleigh criterion states that the minimum distance required to separate two PSFs equals the radius of the first dark ring in the Airy pattern. This value is proportional to the FWHM of the PSF discussed above and equal to 0.5 AU or 1.2 FWHM (box **1**, figures **2a**, **b**, **c**).

depth generally varies from 8, corresponding to 256 (2^8) intensity levels up to 12 and 16 bits, corresponding to 4096 (2^{12}) and 65536 (2^{16}) intensity classes. The increased bit number obviously grants an increased linearity range. However, we should bear in mind that image visualisation on computer screens is usually limited by the monitor's performance and no substantial gain is obtained for qualitative analysis. Real image quantification fully employs this increased linearity range by shifting the saturation limit to higher levels. Spatial resolution of the system is not influenced by bit depth but relies on the number of minimal elements (pixels) into which the field of view is divided (spatial sampling frequency). Each pixel has a physical dimension which results from the spatial extension of the total field of view and the number of recorded pixels (digital dimensions). The field of view depends on the magnification factor of the objective and the zoom factor. In widefield microscopy the physical dimension of a pixel is fixed and relates to the linear extension of the detector and the number of elementary sensor units in the CCD. A 8x8 mm^2 detector area composed of an array of 1000x1000 pixels in a microscope with 100x magnification represents a grid in the specimen with the spacing:

Physical Pixel dimension/Total Magnification =
8 µm/100 = 0.08 µm

To adapt CCD-detector size to the field of view, relay optics are often used, with additional factors of 0.5x ... 2x. This factor has to be included in the calculation for pixel dimensions. Moreover, modern CCD cameras allow pixel binning for noise reduction. Here, the dimension of a single picture element is the size of the binned array. Confocal microscopes allow dynamic variation of the scanned area. This provides an efficient and flexible tool for controlling the spatial sampling frequency, i.e. the pixel dimension.

The size of a pixel must be less than the resolution limit in order to get an image which is really limited by the performance of the optical system employed. We assume a resolving power of 200 nm (depending on the numerical aperture and not on the magnification) and a CCD sensor with a pixel size of 16x16 μm^2. In combination with a magnification of 100x and 2x2 binning, the sampling frequency is 320 nm. The resulting image is then not limited by the optical resolution but by the digitizing system. The Nyquist theorem requests a minimal physical dimension for a pixel to get a real reconstruction of the light distribution sampled by the microscope. This value is half the resolution limit (see insert 2). Theoretically one would expect an increasingly better image when sampling more and more data per pixel (oversampling). However, this also decreases the signal-to-noise ratio and thus the general quality, and consequently the real resolution in the image.

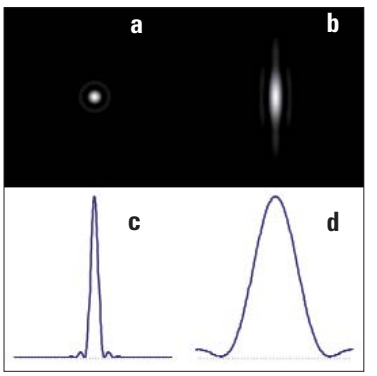

Box **1**, figures **1a – d**: Diffraction and microscopy: Point Spread Function. The PSF of a microscope represents the distribution of the intensity which is created by an object smaller than the resolution limit of the given microscope. The xy-section (a) shows a symmetrical intensity distribution. The corresponding intensity profile is shown in c. The xz-section (b) shows a significant elongation of the intensity profile in z-direction (d). The optical resolution capacity in axial direction is obviously much less than the radial resolution.

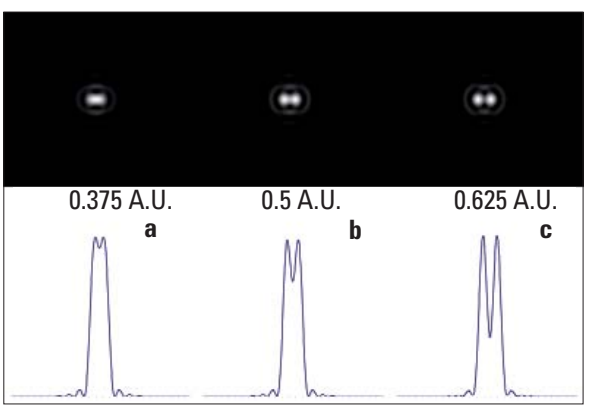

Box **1**, figures **2a**, **b**, **c**: Diffraction and microscopy: Resolution power. The spatial resolution power of a microscope is defined by the minimal distance which is needed to distinguish two point-shaped objects as separated. The figures **2a**, **b** and **c** (xy-intensity distributions and profile through the intensity maximum) show the superposition of two PSFs at a distance below, at and above the resolution limit.

Insert 2: **Optical and digital resolution concepts**

Digital images, recorded both from widefield and confocal microscopes, are arrays of elementary units called *pixels*. The size of a single pixel is equal to the distance between the detection units in the detector when projected into the focal plane. Pixel sizes range from millimeters to nanometers. In a CCD, the pixel corresponds to the area of the photoactive cells that compose the camera chip. This area divided by the total magnification of the microscope provides the pixel size in the object.

In a confocal microscope, each pixel is assigned to a certain position of the laser beam in the scanned grid. Pixel spacing is controlled by the objective magnification and the movement of the scanning mirrors. As the movement of the scanning mirrors is accessible to the operator, the scanning microscope provides additional freedom as compared to the conventional microscope. The physical dimension of the projected laser beam only depends on the numerical aperture of the objective and is entirely diffraction-limited (see insert 1). Assuming an infinite digital resolution, the achieved resolution of the image is controlled by the numerical aperture of the lens. Box **2**, figure **1a**, p.13 shows an example derived from a Fluorescence In Situ Hybridization (FISH) on human fibroblasts to visualize the telomeric sequences of chromosome ends. Each telomere is stained with a Cy3 conjugated DNA probe: excitation is performed at 543 nm, while emitted light peak is positioned at 575 nm (DAPI has been used for the nuclear staining). Panel A shows an image acquired using a 40x oil immersion objective, 1.25 numerical aperture. Pixel dimension is about 45 nm (total magnification factor = 40*8.325 (scanning zoom). The spatial extension (FWHM: see insert 1) of the smallest spot is 260 nm and provides an example of "biological" PSF (the theoretical resolution for the employed acquisition conditions is 0.51*543 nm/1.25 = 220 nm). The same field has been subsequently imaged with a 63x oil immersion objective, 1.4 numerical aperture, with the same final magnification (pixel dimension: 45 nm; total magnification = 63*5.285). In this case the measured FWHM is equal to 220 nm, demonstrating that the image resolution is a function of the numerical aperture of the employed objective.

If the sampling distance is larger than the resolution limit, then the real image resolution is obviously reduced: the smallest distance resolved is equal to the pixel dimension. The real resolution will not increase ad infinitum when the sampling distance approaches zero. The Nyquist theorem requires that the minimal sampling distance is half the optical resolution value in order to record a diffraction limited image.

Box **2**, figure **2** shows the dependence between real, digital and optical resolution as a function of the spatial sampling rate. While the first impression is not dramatically altered by different pixel sizes (a: 75 nm, b: 37.5 nm, c: 150 nm), the measurement reveals a profound dependence on the sampling rate.

Figure **2d** shows the intensity profile of two signals separated by a distance close to the optical resolution limit (ca. 200 nm). A pixel separation of 75nm (Nyquist rate: 100 nm), provided an image where the two telomeric spots were clearly resolved. A further reduction of the pixel size (37.5 nm, figure **2e**) provided a separation identical to the previous analysis. This demonstrates that the increase in the sampling frequency does not produce any advantage in resolution but can compromise the sampling frequency due to higher noise and reduced signal-to-noise ratio.

Figure **2f** shows the result of poor sampling. Due to the pixel dimension of 150 nm (higher than the Nyquist rate) the two signals were no longer clearly resolved.

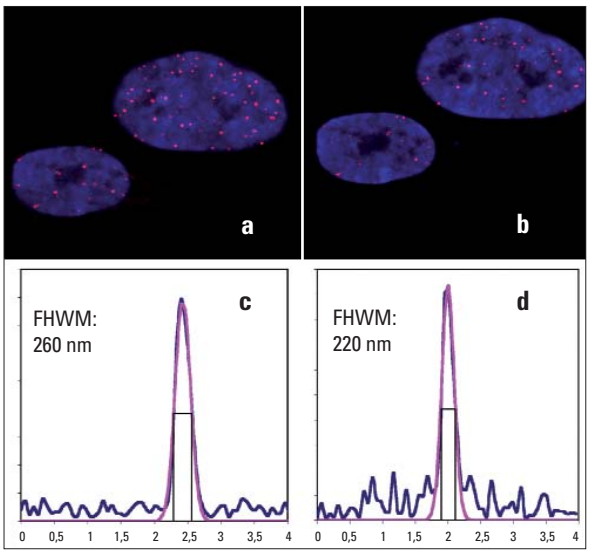

Box **2**, figures **1 a – d**: *Biological* PSF: optical resolution by biological analysis (courtesy of Dr. Sara Barozzi, IFOM-IEO-Campus Milano, Italy). The optical resolution of a microscope in fluorescence depends on the numerical aperture and not on the magnification used. Figures **a** and **b** show images of DNA *in situ* hybridisations of telomeric sequences. The analysis of the intensity profiles presented in figures **c** and **d** reveals the diffraction limited distribution of the signal from telomeres by generating an Airy pattern. Using identical zoom factors (pixel 45 nm), it is possible to show the dependence of the resolution on the objective's numerical aperture (figure **c**: 1.25; figure **d**: 1.4).

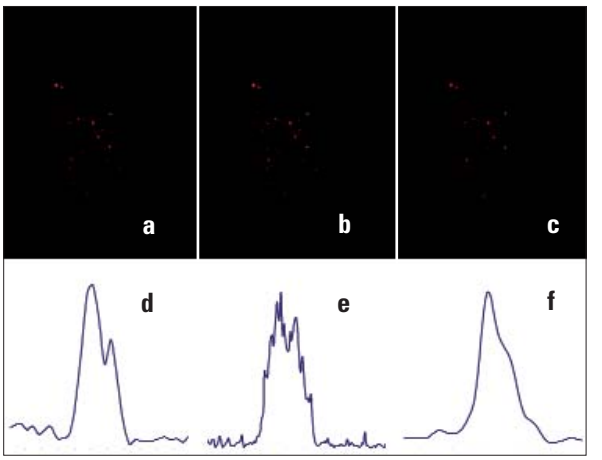

Box **2**, figures **1 a – f**: Optical and digital resolution: (courtesy of Dr. Sara Barozzi, IFOM-IEO-Campus Milano, Italy). The real resolution of an image only coincides with the optical resolution of the microscope if there are appropriate spatial subdivisions (number and physical dimension of the pixels). The analysis of the signal which comes from telomeric sequences shows how the pixel size satisfies the Nyquist theorem. Here, according to the optical resolution, the Nyquist value N was 100 nm. Figures **a** and **c** show results at a pixel distance of 0.75 N, which just allows two different points to be resolved. Using higher zoom values reduces the pixel distance but increases noise. (figures **b** and **c**). The pixel size 0.375 N does not reveal greater detail but reduces visibility due to noise. If the pixel distance is too large, the two points are no longer resolved (figures **c** and **f**, pixel size 1.5 N).

1.2 From Euclid to Descartes: Confocal Microscopy

Widefield fluorescence microscopy provides a two-dimensional view of the three-dimensional world. The widefield setup implies a homogenous illumination in a volume that is determined by the numerical aperture and magnification of the objective, but with a limited depth of focus. As a consequence, the illumination energy does not vary along the optical axis, it is the same in the focal plane and in planes above and below, independently of the z-position. All fluorescence molecules inside this volume will be excited and the emitted photons will be collected. The final image is consequently a superposition of light stemming from the focal plane and light from adjacent planes (figure **4**).

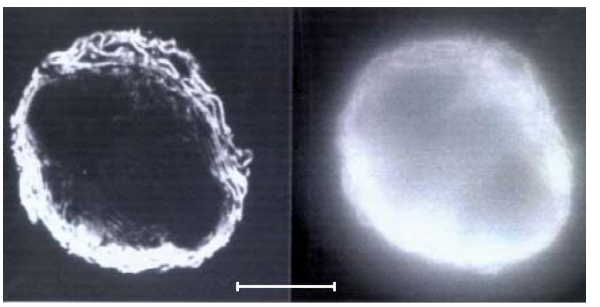

Figure **4**: Conventional and confocal optical microscopy. Image of a plasmacytoma cell stained for endoplasmatic reticulum. Left: confocal image, right: widefield image. The sectioning effect allows structural details of the cellular reticulum to be seen.

As already mentioned, the theoretical optical resolution in the focal plane depends on the numerical aperture of the objective lens and on the wavelength of the emitted fluorescence. The large amount of light from out-of-focus planes can cause a dramatic reduction in the final image contrast. This can decrease the real resolution dramatically as compared to the

expected theoretical value. The real resolution in an image of an isolated point-like object is significantly affected by out-of-focus light when complex samples are imaged. To discriminate diffraction-limited details, fluorescent beads are used as probes. The results from these images cannot be easily extended to the third dimension in complex samples. For example, a measurement of histone H2B-GFP fusion proteins in a 10 µm cell nucleus can produce values quite far from the expected 230 nm. The expected value is calculated with NA 1.4 and an emission wavelength of 520 nm according to the Rayleigh criterion. In such a situation, the focus plane is only 0.3 µm thick and compares to an emitting volume of the entire cell nucleus of 10 µm. This makes it impossible to define a resolution limit along the z-axis.

Laser Scanning Confocal Microscopy solves this problem by introducing two new elements in the instrument setup:

1. The point-like light source is now projected onto the sample in the focal plane of the objective lens.
2. Signal collection is limited to the focal contribution by a pinhole in front of the detector. This variable aperture filters the light spatially and cuts away out-of-focus light from adjacent planes. In this way, an optical section is created.

Since only a point is illuminated, image formation requires a scanning process over the sample. The field of view is covered by physically moving the sample itself, or by moving the illumination spot. Most commonly, a pair of scanning mirrors is used to move the illumination spot. Moving the scanning mirrors allows a variable number of point (pixels) forming the image to be recorded. The field of view is defined by the scanning angle. These two parameters finally define the pixel dimension. Typical digital resolution values for images by confocal microscopes span from 64x64 up to 8192x8192 pixels. In widefield microscopy, fluorescence is induced simultaneously at all points in the field of view. In confocal microscopy the fluorescence is excited sequentially in small areas: each area corresponds to an Airy pattern.

The three-dimensional reconstruction of an object requires a sequence of three steps:

1. Illumination of a point-like area in the sample followed by collection of the signal through a pinhole (pixel collection)
2. Repetition of the first step in order to form a grid of points in the plane (image formation)
3. Movement of the focal plane in the object along the optical axis and replication of the previous steps (stack collection)

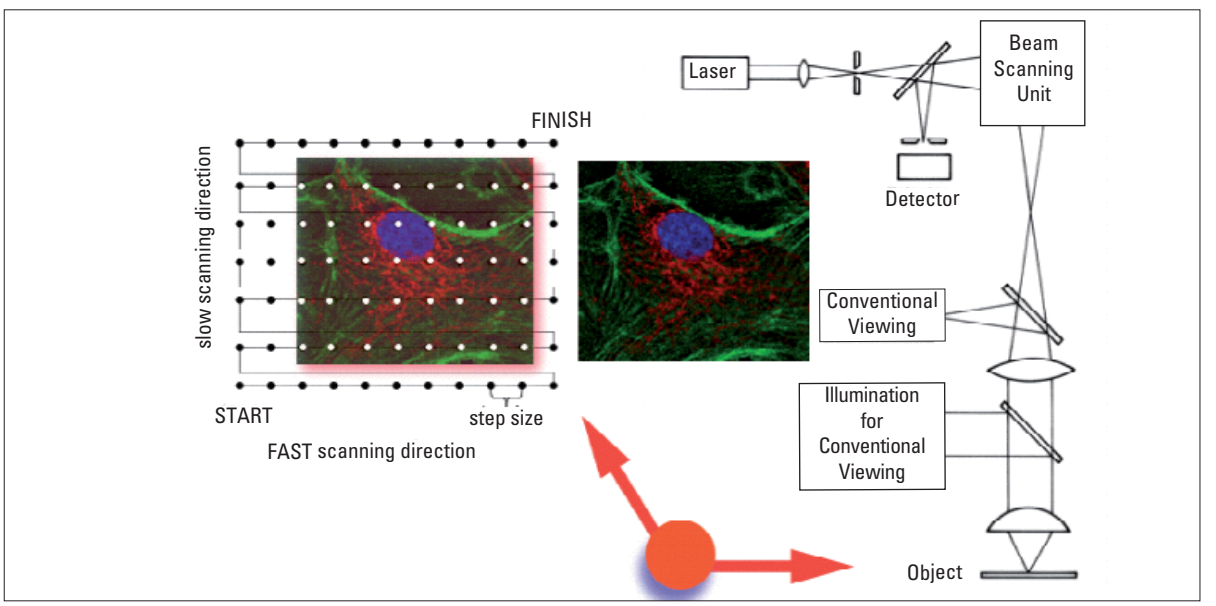

Figure **5**: Confocal scanning microscopy. Image acquisition in a confocal scanning microscope is performed by sequential illumination of point-shaped areas with a focussed laser and successive registration of the induced fluorescence signal. The scheme on the right side shows how an optical system for conventional microscopy has to be modified to work as a system to obtain optical sections.

The stack of images can be projected digitally to provide views from different directions (figure **6**). Here, one has to keep in mind that the confocal microscope is not an isotropic system: the resolving power in z-direction is inferior to the resolving power in the xy-plane. Diffraction-limited objects will be imaged as ellipsoids 2.5 – 3 times longer in z-direction as compared to the circle in xy-directions.

Acquisition of optical sections sacrifices an enormous amount of light by the pinhole through its spatial filtering. The smaller its aperture, the less the contribution from out-of-focus planes. The thickness of the optical section depends on the pinhole diameter and on the emission wavelength. However, setting the right pinhole diameter requires a series of considerations. The optimum is not to close the pinhole as much as possible. If the diameter is too small, the amount of collected light is excessively reduced without any advantage in resolution, but with a huge increase in noise – which ultimately reduces the real resolving power. The optimal value for the acquisition configuration must be deduced from the type of sample in terms of signal intensity, morphology and the goal of the analysis. Larger pinholes can be used for ob-

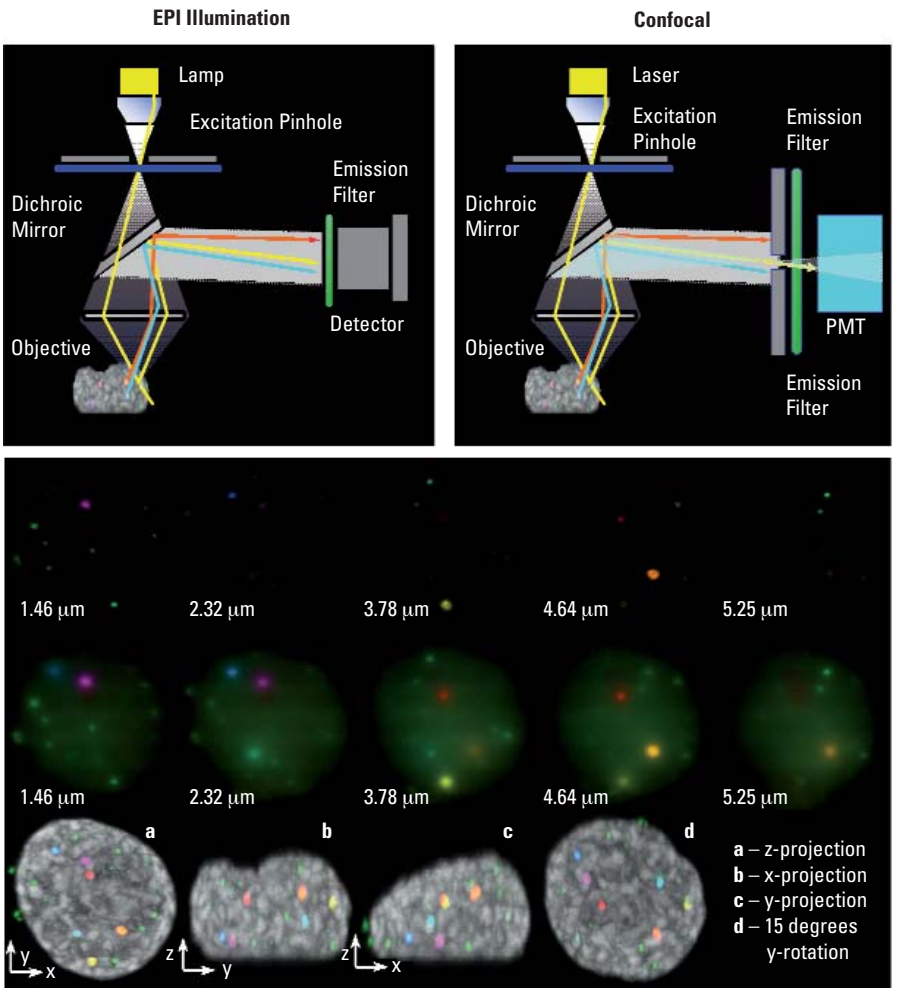

Figure **6**: Optical sectioning. The emission pinhole blocks emission light from layers above and below the focal plane and thus creates a section whose thickness depends on the pinhole diameter, the wavelength of the light and the numerical aperture of the objective. The sequence of images represents a series of focal planes, acquired in confocal and conventional mode (courtesy of M. Marrapodi). The color is a direct staining of PML and a counterstaining for DNA. Each nuclear particle is shown in false colors to indicate the different localizations along the optical axis. The comparison of the two sequences shows the effect of optical sectioning. The lower panel shows volumetric projections at various angles indicating the localization of the signals of the nuclear particles.

serving quasi-two-dimensional samples, such as cell membranes, or very small isolated structures, such as centrioles, than for observing spatially extended structures, such as distributed nuclear proteins.

The pinhole diameter is only one of the factors contributing to the final axial resolution in a confocal microscope. A second element is the spacing between recorded images in a z-stack. As previously mentioned, a laser scanning confocal system offers enormous flexibility in setting the optical zoom, as the extension and the number of points in the scanned field is variable. According to the Nyquist theorem, the proper value is half the theoretical resolution. The same argument applies to the optical axis: at least one half of the axial resolution is required as minimal acceptable distance between optical slices. In the analysis of eGFP light distribution, an efficient value could be set to 80 nm, assuming radial resolution of 160 nm. In axial direction, the resolution is 560 nm, and the optimal spacing is therefore 280 nm. The scanning mirrors in confocal microscopes allow much smaller values in xy, but it is important to keep in mind that the fluorescence will bleach in a square mode to the optical zoom. Since the optical sectioning is the result of spatial filtering of the emission, a large portion of the sample is illuminated every time an optical section is collected. This causes extensive photobleaching both inside and outside the observed plane during stack collection. Consequently, excessive (over-)sampling in the focal plane or along the optical axis can cause uncontrolled photobleaching with an associated loss in signal-to-noise that determines the real image resolution.

Another fundamental factor controlling spatial sampling is related to the goal of analysis. Let us assume that we are observing very small structures close to the diffraction limit, for example centromeres or a portion of the mitochondrial network or an eGFP tagged nuclear structure. The Nyquist theorem requires 80 nm pixel size for an *informative* zoom. Assuming a physical size of 800 nm, the digital dimension of the structure of interest (e.g. an isolated mitochondrion) is then only 10x10 pixels. A software based zoom to produce print-quality images for publication will show an evident pixelation. Here, an increase of optical zoom during image collection can help to obtain a better appearance strictly from an esthetic point of view. It is important to keep in mind that no additional information or resolving power is added to the image, which remains diffraction-limited. From the discussion above, we learn that the confocal microscope has a better resolution than a widefield system. The increased resolution has to be maintained by optimal settings of the acquisition parameters, which also need to consider adequate signal-to-noise ratio.

The signal strength in images taken with a widefield microscope reaches extremely high values, as the exposure time can be very long and consequently the number of collected photons is high. In a confocal microscope, this feature is lost in favour of spatial resolution. Here, the pixel dwell-time, i.e. the time interval spent by the laser in a certain position, is in the range of microseconds. This characteristic made the confocal very similar to another fluorescence-based optical system: the flow-cytometer. In flow-cytometry, signal collection is limited to the time interval in which cells cross the laser beam. The situation is consequently similar to what happens in a confocal microscope, but in a reverse manner: the laser beam is fixed and the sample moves through the spot. Due to this similarity and other common instrumental and functional features, confocal microscopy was in the past referred to as *static cytometry*.

Once the *exposure time* is fixed by setting the scanning speed, the parameter for varying the number of collected photons is the illumination energy. Contrary to widefield microscopy, where the excitation intensity is not usually modified, in a confocal microscope the excitation energy is continuously variable. Optimal signal collection then requires balancing the illumination intensity against the electronic gain of the detectors to maintain an acceptable signal-to-noise ratio. As already mentioned, the pinhole aperture also controls the collected photons: a lower spatial filtering could yield better contrast and in consequence a better real image resolution despite the common belief that an increased optical slice thickness is necessarily accompanied by worse resolution.

The term *confocal* indicates a significant difference to the widefield technique. People frequently think that the two systems become equivalent when the pinhole is absent or fully opened. This would indeed make the two optical systems similar, as far as sectioning ability is concerned (or rather the loss in optical sectioning capability), though resolving power

is not equal in both systems. Focussing of a point-like source on the sample and the consequent scanning procedure in confocal microscopy gives per se an increased spatial resolution as compared to conventional fluorescence microscopy.

Although confocal microscopy shows exceptional analytic capabilities, it is not a cure for all problems. The choice between the two techniques must be made carefully, always considering the experimental conditions in order to avoid erroneous estimations in performance. In 1870, Hermann von Helmholtz, a superb expert in physiology, physics and mathematics, proposed: "Let us consider for a moment – it is logically not impossible – a species of thinking beings, living and moving on the surface of a solid body. Let us suppose that they cannot feel anything outside this surface, but they can feel, like we do, the reality on the surface where they live. If these beings built their geometry, they would obviously attribute to the space two dimensions only". These words obviously inspired Edwin Abbott to create *Flatlandia*, a tale of a world in two dimensions populated by the figures of Euclidean geometry. Let us suppose for a moment that one day the "square", principal player of the Flatlandia story were to enter the collection of samples to be analyzed in your laboratory: Would you choose widefield or confocal microscopy to examine this peculiar sample?

1.3 From Descartes to Einstein: Live Cell Imaging

The introduction of the temporal dimension in fluorescence microscopy greatly increased the range of applications in cellular biology. The hereby induced revolution for quantitative biology is comparable to the effect of the formulation of the spatio-temporal universe in Albert Einstein's theory of relativity, which opened the way to a better comprehension of cosmological and subatomic space in modern physics. The real revolution for fluorescence microscopy resides in the possibility to follow biological events almost at the same speed as the biological processes (see figure **7**).

This fundamental step is not just a result of modern computer technology that allows a computer to be taught to control a microscope to record data at fixed time intervals. Time lapse experiments in life cell biology require optimal configuration which is different from configurations for observation of fixed samples. Sometimes the optical system has to be modified as well. The new parameter in the universe of the observed variables introduces the concept of temporal resolution, the ability to distinguish separate events on the time scale. Laser scanning confocal microscopes are limited in acquisition speed due to the point-by-point image formation process. Typically, the speed for acquiring standard images (512x512 pixels) is in the range of a few frames per second – an extremely low value if compared to the speed of biological events such as e.g. Ca^{2+}-fluxes, to cite just the most famous. Here, conventional microscopy performs better thanks to the parallelization in image acquisition. The temporal resolution of scanning systems has been greatly increased by the introduction of a new class of instruments between widefield and confocal microscopy using parallel scanning procedures. Here, the acquisition speed is dramatically increased at mod-

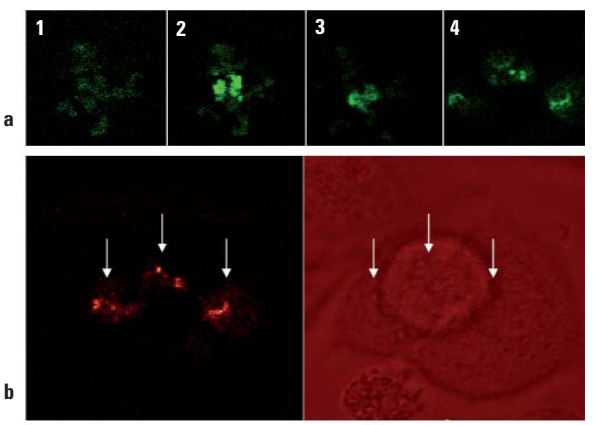

Figures **7a, b**: Live Cell Imaging. Confocal microscopy applied to studies on cell division. HeLa cells transfected with a fusion of paGFP-histone H2B. The paGFP is a variant of green fluorescent protein (GFP). PaGFP can be activated for photo tracking processes (see chapter on FRAP). When expressed in the nucleus, the fusion-protein moves into the chromatin and stains the metaphase plate in mitosis (figure **7a**, record **1**). Illumination with 405 nm highlights a selected region by inducing a strong fluorescence (record 2). The mitotic process can be followed in time from the origin to the daughter cells (records 3 and 4). Figure **7b**: Fluorescence image (left) and transmission image (right). Courtesy of I. Testa (LAMBS, Genova), S. Barozzi (IFOM-IEO, Milano)

erate cost to spatial resolution. The sample is illuminated at multiple positions with fixed spacing in order to avoid too much light interference. This concept is realized in Nipkow-disc confocal scanheads and in line scanning systems, where the sample is scanned over a full line.

Obviously, the selection of the right solution requires a compromise between expected spatial and temporal resolution. For example, reduction of image dimensions (pixels per line) in a confocal microscope provides better time resolution, but decreases spatial information. The spatial information is either lost by reducing the field of view and scanning correctly for maintaining spatial resolution, or by reducing the real resolution in larger fields of view. These considerations are obviously valid for all spatial dimensions when the analysis is extended to samples that require optical sectioning (and thus a confocal microscope). At the extreme, the image may consist of only a single line, which then allows temporal resolution in the millisecond range (xt-mode).

In the previous chapter it was mentioned how acquisition settings can cause significant differences between theoretical and real resolution. This is even more pronounced in live cell microscopy, as the environmental conditions often do not match the requirements for optical analysis. Normally, a fixed sample is mounted in specific mounting media required to avoid spherical and chromatic aberrations. These media also contain anti-fade agents to reduce photobleaching and other substances. The cell medium is instead an optically active element which can cause degradation in image resolution. Light scattering and photon emission by fluorescent molecules induce a high background level. Significant optical aberrations are also introduced by index mismatch when lenses with high numerical aperture and oil immersion (n = 1,52) are combined with living samples mounted in aqueous media (n = 1,33). Special objective lenses for glycerol or water immersion account for this problem.

Although a better signal-to-noise ratio might be gained when the illumination intensity is increased, this causes not only photobleaching but also phototoxic effects. High energy excitation in the molecules produces free radicals of an extremely reactive chemical species. They can modify cellular components causing significant damage – even cell death. Living cell analysis is therefore affected by a problem similar to the famous paradox of *Schrödinger's cat* in quantum mechanics. This most famous pet of modern physics lives enclosed in a box completely isolated from the external world. A poison vial is connected to the box cover and an attempt to lift the cover will cause damage to the vial– immediately killing the animal. How can anybody know whether the cat is still alive without removing the cover of the box?

It seems that fluorescence microscopy, when reaching the fourth dimension, faces the same problems as modern physics at the same point. The solution may require accepting – at least for the moment – some kind of uncertainty principle for optical microscopy. To obtain analysis conditions compatible with life, it is necessary to compromise between spatial and temporal resolution – without impairing the reliability of the experimental observation by deranging the living system.

1.4 From Einstein to Superstrings: Spectral Confocal Microscopy

The above mentioned similarities between the evolution of modern microscopy and the history of physics end here with the capability of both to surpass the common perception of the world around us. Both introduce additional dimensions to better explain the natural phenomena and the laws beyond them. To be more precise: the physical theories based on the concept of superstrings propose the existence of 10 dimensions! These theories have been introduced to obtain a unified vision of the universe from the subatomic to the cosmological scale. Modern microscopy has crossed the frontier of four dimensions by introducing the spectral dimension. Characterization of fluorescence now includes measurement of emission intensity, the spatial position, temporal changes and finally the entire spectrum of wavelengths as emitted upon excitation at a fixed energy. It also includes final analysis of the photophysics of the event. Before discussing the advantages and applications of such a revolution, it is advisable to take a closer look at the engineering of an optical system which is able to perform spectral analysis. The optical sectioning capability of a confocal system is a result of the pin-

hole in front of the detectors. Similarly, spectral sectioning, i.e. the capability to classify the collected light in the composing wavelengths, is established by the introduction of a dispersive element in the scanhead (figure **9**).

The phenomenon of light dispersion, whose brilliant theoretical basis was founded by Sir Isaac Newton in the late 1660s when experimenting with his *celebrated phenomenon of colors*, implies the separation of the different chromatic components by basic optical elements such as prisms or diffraction gratings. Applying these elements in a confocal microscope setup allows analysis of the emission spectra of fluorescent molecules. The term spectral resolution usually refers to the minimal interval that can be measured over a range of wavelengths. Current spectral systems offer resolution from a maximum of 10 nm to a minimum of 2 nm. The spectral dimension does not represent an exception to the limitations discussed so far regarding the potential discrepancies between theoretical and real resolution of a system. Here too, the optimal sampling can be compromised by an insufficient signal-

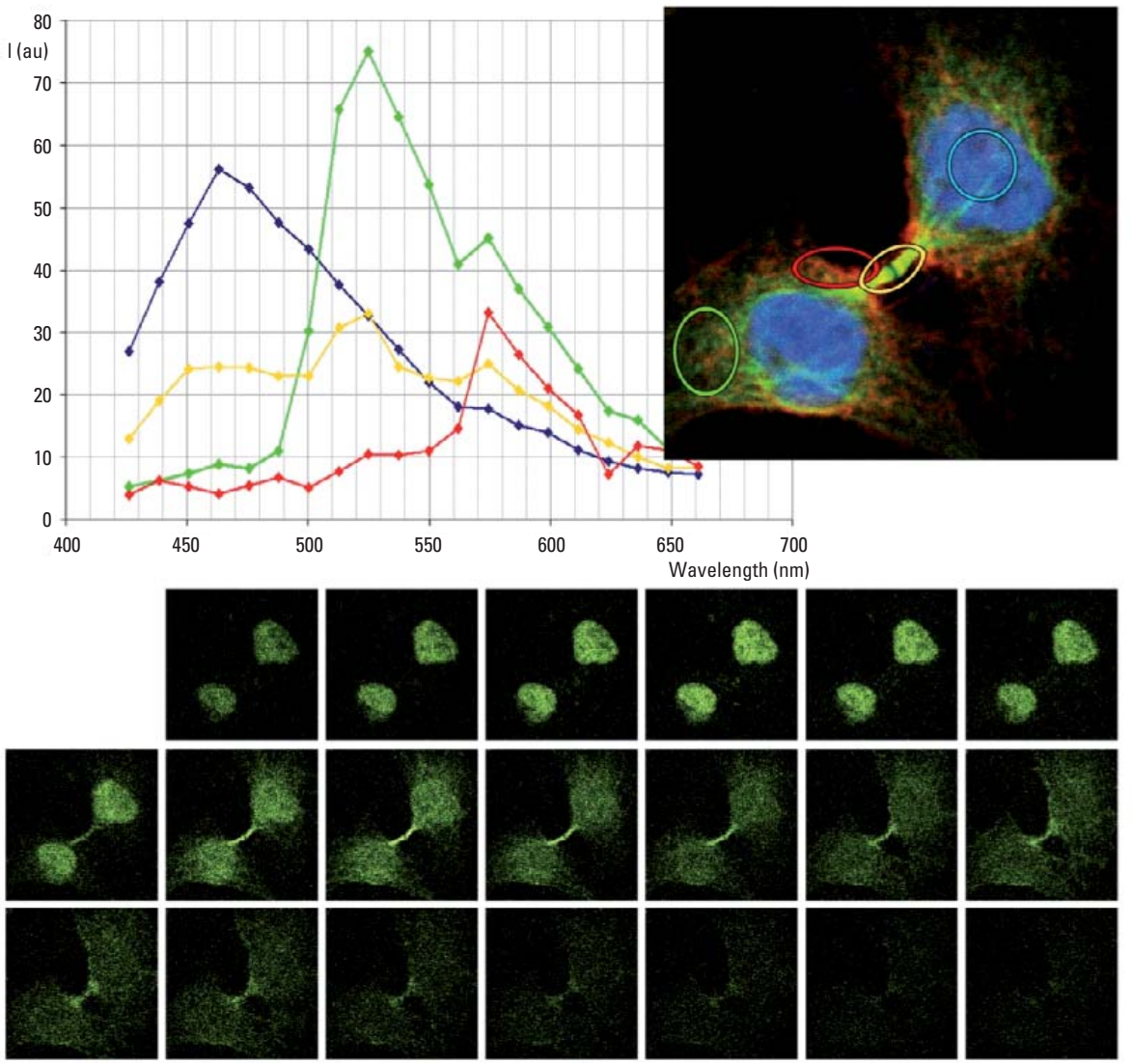

Figure **8**: Confocal scanning microscopy with spectral analysis capabilities. Example of spectral scanning applied to an area of multiple fluorescence staining. The sequence of images shows the signals in different spectral intervals in the range of 425 – 660 nm. The graphical analysis of different regions of interest of simultaneously recorded fluorochromes shows the individual contributions from the fluorochromes. (courtesy P. Bianchini, LAMBS, Genova)

to-noise ratio due to a low number of photons over the background. Sometimes the separation of two different emission spectra can be efficiently enhanced by a lower spectral sampling if associated with increased contrast in the collected signal.

The ability to measure spectral properties of fluorescent molecules grants a high degree of flexibility in fluorochromes and a maximum number of simultaneous combinations. The setup of a microscope equipped with dispersive elements allows configuration of optimal emission bands, which is important for efficient separation – a condition which is not so easily met in filter based systems. However, the crosstalk between emission from different fluorophores is caused both by a partial superposition of the emission spectra and by an overlap in excitation and emission properties.

The most commonly employed method for emission separation is based on sequential excitation (and collection) of the fluorochromes. If excitation spectra are sufficiently separated, this sequential recording is an efficient tool for distinguishing different fluorescent molecules even in the presence of a significant overlap of the emitted fluorescence. However, excitation tails – even if looking marginal on the paper – can cause relevant crosstalk when signal intensity is strongly unbalanced. In this case, the sequential excitation is not sufficient to obtain a good separation. A solution might be

- choice of spectral bands in regions where the emission does not show any overlap
- spectral signal collection over an extended interval in order to collect enough information to separate the fluorescences by computational techniques (spectral unmixing)

Measurements of fluorescence spectra not only represent an invaluable tool for obtaining correct spectral separation, but also allow characterization of emission properties of endogenous fluorescence. Let us consider biological tissues, for example. The molecular components of a living animal (haemoglobin for example) or plant (chlorophyll) tissue possess precise photophysical properties that can be measured by a spectral confocal microscope in order to characterize the sample composition and its functional properties.

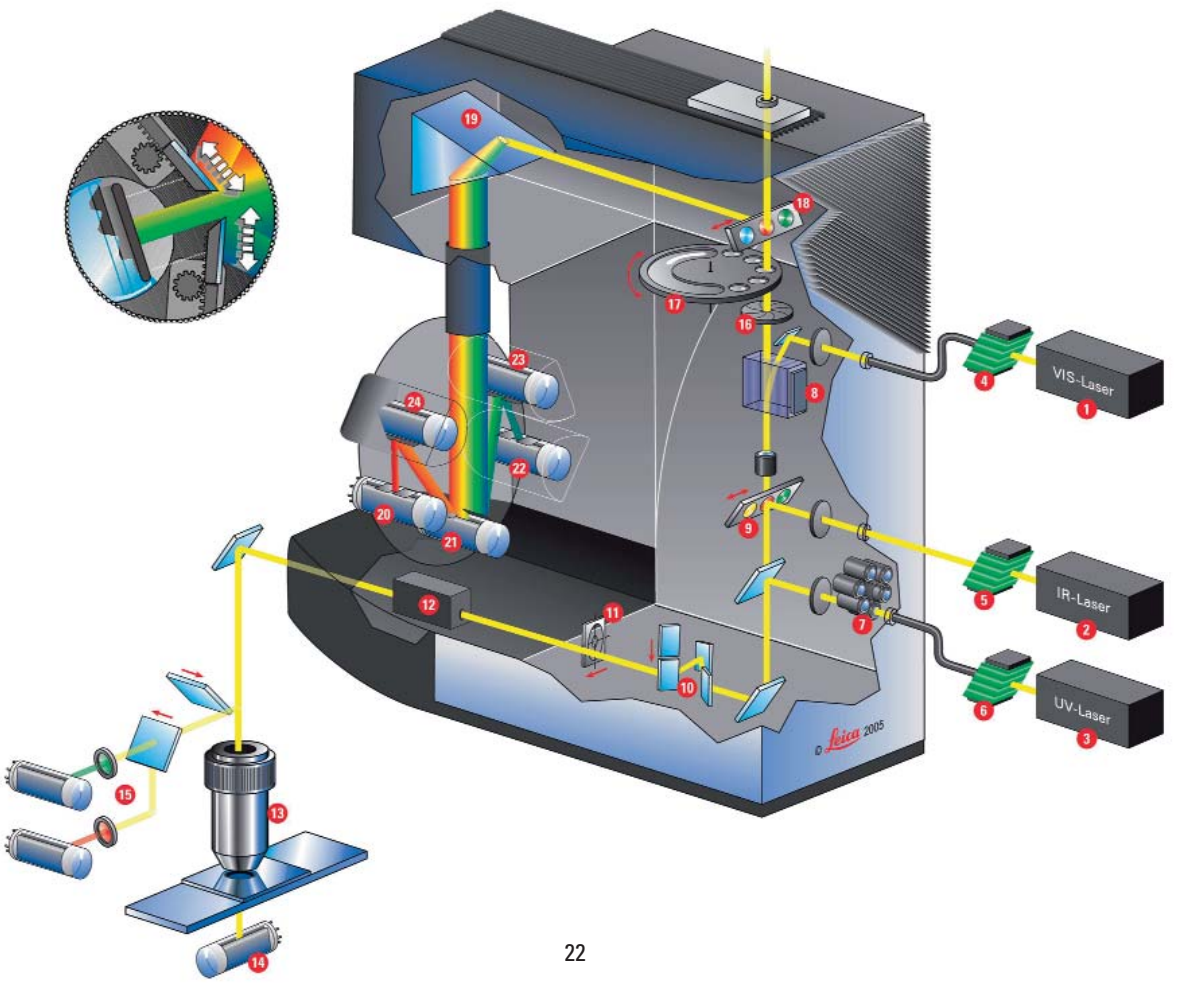

Insert 3: **Biological Applications Using Spectral Confocal Microscopy**

The integration of a dispersive element in the confocal scan head opened the way to dynamic selection of the collected emission band to further increase the potential of confocal microscopy as a research tool in biomedicine. The possibility of individually defining the spectral range of the collected light for each channel separately dramatically increases the efficiency in signal separation as compared to classical optical filter based systems.

The Box **3**, figure **1**, p. 22 shows an example of a four parameter staining for analysis of the spatial localization of Sgt1 protein in relation to different cellular compartments: actin cytoskeleton stained with FITC conjugated phalloidin, mitochondrial network marked by DiOC6 green emitting dye and cellular nucleus stained with DAPI. The DiOC6 and phalloidin-FITC show a partial overlap in absorption and emission. A sequential acquisition with appropriate setup for collection of the spectral intervals (DiOC6: 500 – 520 nm; FITC: 560 – 590 nm) ensures efficient separation of the two fluorescence signals. Besides the flexibility to collect tuneable emission bands, spectral systems are equipped with software tools for reconstruction of the original signal distribution in space and spectrum from lambda-scan data. The Box **3**, figure **2**, p. 22 shows a 5-parameter fluorescence analysis of a histological tissue section (human intestine). The localization of selected proteins has been analyzed in comparison to known morphological or molecular expression markers. In order to use a higher number of parameters, it was necessary to use fluorescent dyes with overlapping spectral properties. TRITC conjugated phalloidin staining endogenous actin and Alexa 568 staining the PML protein have very similar emission spectra, as shown in figure **2b**. The emission spectra have been recorded in samples stained alternatively with only one of the two markers. A spectral scan with 5nm steps in the interval 550 – 620 nm was sufficient to get a good separation of the two signals by an unmixing procedure (figure **2a** and **c**). It is important to use spectra measured in the sample and not taken from tables in literature on the subject, as photophysical properties may dramatically depend on the sample and preparation protocols (acidity, autofluorescence,...)

The Box **3**, figure **3**, p. 20 shows an additional example of how to use emission spectra in confocal microscopy: the analyzed signal is the autofluorescence in mouse mammary tissue sections when exposed to 488 nm light from an Argon laser. Spectral analysis showed how the autofluorescence overlaps with the emission spectrum of a green emitting fluorochrome (magenta curve: fluorescein). This gives a hint for selecting more efficient immunostainings; in this case for using a dye emitting in the red or far red spectral region, e.g. TexasRed, Alexa 568 and/or Cy5.

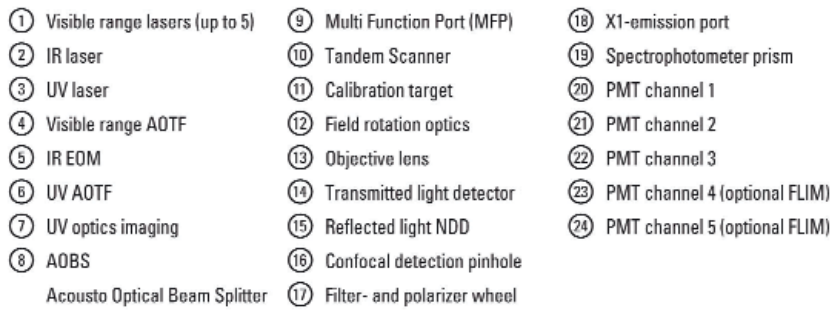

Figure **9**: Confocal Laser scanning head with spectral capabilities. The fluorescence emitted from the sample passes the scanning mirrors, is separated into its chromatic components by a dispersive element (prism) and reaches the different photomultipliers. The slit precisely positioned in front of each detector allows the selection of exactly defined spectral intervals (p. 20).

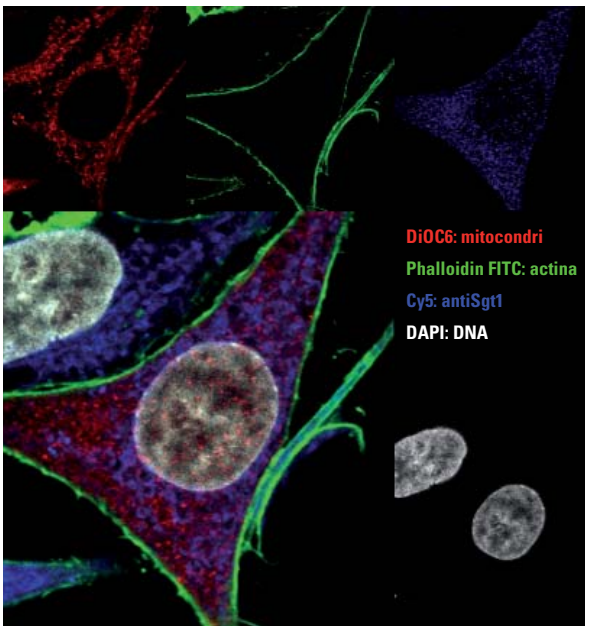

Box **3**, figure **1**: Spectral microscopy: example of optimization of multiparameter acquisition. The capacity to resolve spectrally allows modulation of the acquisition windows for multiple fluorochromes. This results in optimal separation of the emission signals. (Courtesy of A. Musacchio, P. Steensgard and M. Garre; IFOM-IEO Campus, Milano)

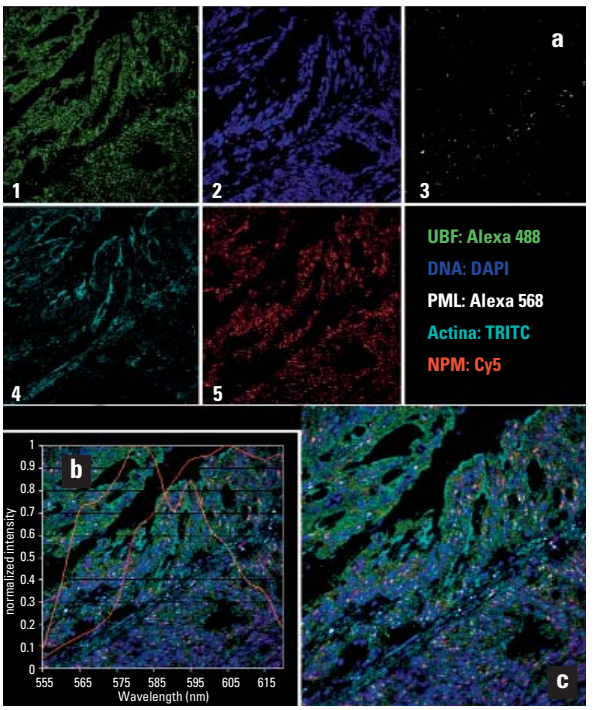

Box **3**, figures **2a, b, c**: Spectral microscopy: spectral deconvolution for separation of the signals of multiparameter recordings. The recording of information on the distribution of the signal (figure **b**) allows the application of appropriate algorithms to extrapolate the correct distribution of fluorochromes with strongly overlapping emissions (Alexa 568 and TRITC, figure **a**). This makes it possible to acquire a higher number of parameters (figures **a** and **c**), which is very difficult with filter based confocal microscopes.
(Courtesy of P. Transidico, IFOM-IEO Campus, Milano)

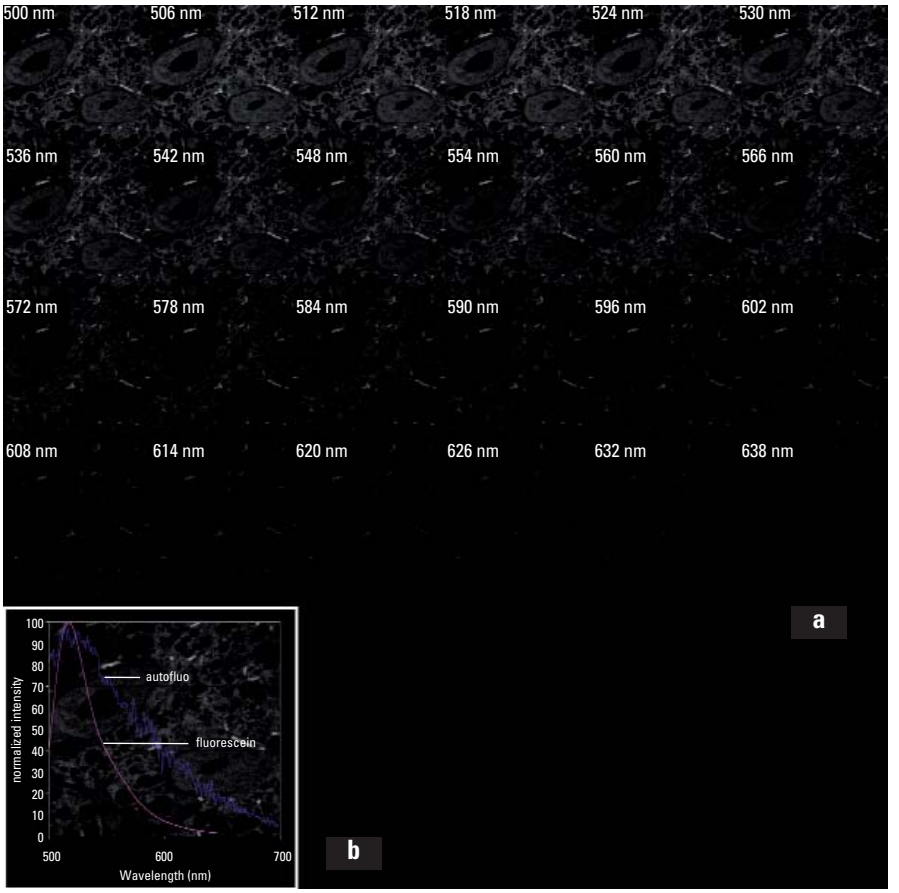

Box **3,** figures **3a, b**: Spectral microscopy: spectral analysis for photophysical characterization of biological samples. The recording of a spectral sequence (figure **a**) allows the characterization of autofluorescence signals in biological samples. This is important when selecting the colors of specific markers. Figure **b** shows the strong emission of the autofluorescence in the green range (blue curve) compared with fluorescein (magenta curve) indicating that it is better to use red emission dyes for specific stainings. (Courtesy of G. Bonizzi and A. Cicalese, IFOM-IEO Campus, Milano)

2

2. From Structure to Function: Fluorescence Recovery After Photobleaching (FRAP) and Fluorescence Resonance Energy Transfer (FRET)

To understand the complex mechanisms that regulate life, all sciences engaged in this challenge use a common approach. Starting from the structural analysis of the elementary components, it is then possible to translate that information into functional concepts about their role in the complex network of interactions in cells or in organisms. Optical microscopy is an excellent tool for structural analysis thanks to its low invasiveness and high resolving power. The ability to analyze living objects without substantially interfering with their metabolic processes made optical and, in particular, confocal microscopy a potential tool for functional characterization of molecular events. New assays based on fluorescence microscopy allow monitoring of chemical reaction dynamics of biological macromolecules, characterization of physical parameters of the cellular microenvironment and measurement of the spatio-temporal process of molecular interactions. The following chapter presents an overview of the most frequently used analytical techniques and explains the underlying principles. It also discusses the main technological features and describes the data analysis and evaluation protocols for extracting the biological information.

2.1 Fluorescence Recovery After Photobleaching (FRAP): "And yet it does move..."

Photobleaching irreversibly switches off fluorescent molecules and it is a well known phenomenon in all fluorescence applications. However, photobleaching can be employed to measure molecular dynamics by a technique called Fluorescence Recovery After Photobleaching (FRAP). In a FRAP protocol, the fluorescence inside a defined region is destroyed by a high intensity laser source. On a fixed sample this operation simply results in a dark spot. In living cells, the molecular mobility can refill the bleached areas with new fluorescent molecules. This causes a reconstitution of the signal in the previously bleached area. The speed of the recovery provides a measurement of the dynamic properties of the molecular species in the sample under examination.

The entire process can be divided into three main phases:

- Prebleaching: Recording of images in order to measure fluorescence intensity $F_{(pre)}$ in specific regions of interest, e.g. a cellular compartment.
- Bleaching: Illumination of the region of interest with high energy density to induce fluorescence decay until a predefined value $F(0)$ is attained.
- Recovery: Monitoring of the fluorescence intensity F(t), ideally until a new equilibrium $F(\infty)$ is achieved.

The ratio of the recovered signal at the time t and the equilibrium corrected by the initial value

$$\frac{F(t)-F(0)}{F(\infty)-F(0)} = f(t, t_{1/2})$$

can be modelled with appropriate functions $f(t, t_{1/2})$ where $t_{1/2}$ provides an estimate of the speed of the process. The type of f is based on the nature of the observed data and may have different degrees of complexity. The physical interpretation of the parameter $t_{1/2}$ is consequently variable, for instance it is associated with a diffusion coefficient or with a dissociation rate of a chemical reaction. Usually $f(t, t_{1/2})$ is adequately represented by a weighted sum of exponential terms.

The quantity

$$\frac{F(\infty)-F(0)}{F(pre)-F(0)}$$

describes the mobile fraction of molecules inside the analyzed region: the recovered signal (numerator) is lower than the original value (denominator), if a part of the fluorescence in the bleached area is bound, and only the free moving fluorochromes will contribute to the recovery. The fluorochromes which do not move are called *immobile fraction*. The FRAP application is based on the fundamental assumption that the total amount of fluorescence in the sample is much larger than the bleached fraction. Otherwise the recovery signal is ambiguous.

The evaluation of molecular mobility in large compartments is usually based on a different experimental protocol called FLIP (Fluorescence Loss in Photobleaching). Here, a region of

interest is repeatedly photobleached and the signal outside the region is continuously recorded. If there is transport into the bleached compartment from outside, one can measure an increasing decay outside the region. A typical application is the analysis of transport from cell nucleus to cytoplasm. The performance of a FRAP or FLIP experiment depends on optimal settings for pre-bleach and post-bleach time intervals and the right choice of instrument parameters.

Correct results require minimal perturbation of the sample during the entire experiment. Here, good compromises have to be found for high frequency and long term sampling to obtain reliable data both for pre-bleach and post-bleach measurements. On the other hand, one should restrict the number of exposures as much as possible to reduce unintended bleaching. Setting of instrument parameters (laser intensity, pmt-gain, averaging, zoom factor and so on) have to be delicately tuned to reduce perturbations but still provide a high signal-to-noise ratio. (See also the Live Cell Imaging discussion in the previous chapter).

The sampling frequency (frame rate) is critical in FRAP experiments. On one hand, the acquisition speed has to be sufficiently high in order to collect gapless data, on the other hand the noise level must be kept low as otherwise the data analysis would fail. Furthermore, the bleaching caused by recording data in the recovery phase has to be reduced as much as possible. If there is residual bleaching during data acquisition, this has to be taken into account for analysis, requiring sufficient data for an estimation of this decay. Photobleaching is easily monitored by analysis of regions outside the FRAP region, e.g. a different cell in the field of view. Numbers acquired from these measurements can be easily assigned to FRAP measurements.

A critical point in the entire process is the bleach phase. During bleaching, data recording is not possible, as the high energy for bleaching causes the detectors to overflow. Therefore, the bleaching phase should be very short but without mitigating the spatial confinement. The confinement can be achieved by various methods. The first uses the ability of the confocal microscope to zoom in, reducing the extension of the scanned field to a region of interest. The reduction of the field of view with an unaltered spatial sampling frequency implies an increased delivered energy density and consequently a better bleaching efficiency. Arbitrarily shaped regions of interest require the employment of an acousto-optical device (AOTF: Acousto-Optic Tunable Filter). With these crystal devices, the excitation power can be varied on an extremely rapid time scale. Thanks to this tool, which is available with almost all confocal microscopes on the market, the illumination energy can be controlled in every single point, which allows the use of maximum power on arbitrarily shaped regions. Here, no zoom variation is required and one can image a full field, e.g. show an entire cell and selectively inactivate the fluorescence in a specific compartment with full laser power during scanning. However, the delivered energy depends on the zoom factor, and the above described solution might not be sufficient for applications where photobleaching is too slow at the energy level employed. In many cases, the optimal photobleaching protocol is a mixture of region-of-interest bleaching by AOTF in conjunction with field variation by zoom.

The required bleaching speed depends on the speed of the transport processes analyzed. When the exchange of fluorescently labelled molecules is faster than the decay of fluorescence in the region of interest, obviously no recovery is observable. The continuing replacement of fluorescent molecules in the bleached area during extended bleaching times will cause a reduction of the fluorescence intensity in the whole cell. This phenomenon can easily be observed in a biological environment, when looking at the GFP motions inside a cell. Due to diffusion of the protein, it is impossible to locally bleach the fluorescence; and in turn, the fluorescence of the whole cell fades away.

Finally, the analysis of FRAP processes also requires some considerations on optical sectioning in confocal microscopes. In order to record recovery information at high time resolution, data acquisition is done in a single focal plane that contains the region of interest. Most analysis procedures are based on fitting of two-dimensional models to the data. The optical section is achieved by spatial filtering through a pinhole, which cuts away out-of-focus emission. But excitation is not limited to the focal plane and causes bleaching above and below the focus as well. In a confocal microscope the excitation is not confined to three-dimensions, and a bleach experiment in the basal membrane will also cause bleaching in the apical membrane (in the respective defocus area). A 3D

confinement for excitation can be obtained by multiphoton excitation, where nonlinear absorption inherently causes a limited excitation in the focal plane (see chapter **3**).

Special care has to be taken for the analysis of the FRAP data. Correct evaluation of the measured data is based on correct modelling of the experimental procedure by ad-hoc assumptions. As previously mentioned, the analysis requires the temporal dependence of the fluorescence recovery to be fit to a function $f(t, t_{1/2})$. It is tempting to refer to the function f as a universal definition, attributing to the parameter $t_{1/2}$ (and other eventually introduced parameters) an invariant biophysical meaning. It is, though, important to note that such a coefficient essentially measures the speed of the process, without any reference to the shape of the chosen fit function. According to the observed sample, $t_{1/2}$ could provide a measure of a diffusion coefficient inside a specific compartment, as in the studies of the lateral diffusion events in cell membranes, or be linked to the half-life of a molecular complex, as in the analysis of chemical reaction kinetics of fluorescently tagged purified molecules.

Biological processes are typically the result of a mixture of reaction and diffusion events. The correct evaluation of FRAP data must take into account potentially hidden parameters. It is possible to define in vitro the nature of a chemical interaction by measuring the dissociation rate and, consequently, the half life of a molecular complex. The translation to the cellular environment is, however, not always a simple task as other factors, e.g. concentration and viscosity, can modify the interpretation of the measured data. Numerically comparable results might represent extremely different biological scenarios due to the complexity of the events analyzed. Nevertheless, even if absolute quantification is limited by unknown parameters, a qualitative interpretation can still provide useful information allowing discrimination between ordered molecular fluxes and purely diffusive phenomena. Since ordered motion is energy driven, an ATP deprivation can consequently alter recovery kinetics and provide initial evidence on the mode of the process.

To complete the overview on fluorescence recovery after photobleaching techniques, a comment on photoactivation is necessary. Photoactivation techniques show remarkable similarities with FRAP: the activation of the non-fluorescent molecule into a fluorescent molecule requires exposure to high energy fluxes for structural conversion. One of the best known photoactivatable molecules is paGFP, a point mutation of the GFP protein. paGFP exhibits extremely dim fluorescence when illuminated by 488 nm in its native form. Activation by 405 nm light causes a modification in the excitation spectrum and increases the absorption at 488 nm with significantly increased emission when excited at this wavelength. To selectively activate a specific region of interest for the photoactivation procedure, similar considerations hold as described for photobleaching. Selective marking of e.g. the mitochondrial network by photoactivation allows the dynamics of intracellular trajectories to be followed or cellular subpopulations inside complex organisms to be identified, such as progenitor cells during embryonic development.

Insert 4: Fluorescence Recovery After Photobleaching (FRAP) protocols introduced an extremely powerful tool to the study of the localization dynamics of biological molecules. The following figures present examples of qualitative analysis on nuclear compartmentalization. In particular it is possible to extrapolate information on the stability of the examined structures, distinguishing between a *self-assembled* or *self-organized* compartment.

Box **4**, figure **1** displays the cellular distribution of a chimeric GFP-PML (ProMyelocytic Leukemia) protein. The fusion protein is localized in nuclear bodies, called PML Nuclear Bodies, of variable dimension (figure **1a**). The selective bleaching of one of the nuclear bodies (green circle) evidenced their "static" composition, indicating PML as a permanent "structural" component of this self-assembled structure. The panel B graph shows a modest percentage of recovery (20 – 30%) on a very long time scale (10 min). The stability of a second not irradiated nuclear body (magenta circle) demonstrates very low photobleaching due to the imaging conditions in the recovery phase.

Box **4**, figure **2**, reports an example of high molecular mobility linked to functional interactions. Cells over-expressing the

GFP-p53 (green) and CFP-PML (red) fusion proteins presented a pattern characterized by an expected accumulation of p53 in the PML NBs, the latter molecule being a well known PML interactor. The targeted bleaching of the GFP signal in the PML NBs revealed a continuous flux of molecules sustained by the high chemical affinity existing between the two molecular species: the GFP fluorescence recovered to more than 70 % of the initial value in about a minute ($t_{1/2}$ ~ 20 sec). Box **4**, figure **3**, shows an additional example of correlation between spatial localization and molecular mobility. The GFP molecule has been targeted to the nucleolus by the fusion with a specific nucleolar localization signal. Once the nucleolar binding sites have been saturated the chimeric constructs localized in the nucleoplasmic compartment (figure **3a**: Colored rendering of the signal intensity. White-magenta for high and green-black for low concentrations).

The study of the molecular mobility inside the nucleolus (blue curve and arrow) evidenced the presence of two different dynamical components, with a fast recovery in the order of 10 – 20 seconds, and more static ones corresponding to a immobile fraction of about 50 %. Monitoring of a second cell in the field of view allowed quantification of the imaging photobleaching rate, ensuring a very low photodeacay during the recovery phase (red curve and arrow). The bleaching of an extended area altered the global fluorescence, providing qualitative information on the overall mobility at nuclear level. Monitoring of a second nucleolus and of the nucleoplasmic component in the bleached cell showed a relevant reduction in the diffused nuclear signal (light blue curve and arrow) in contrast to slightly altered intensity in the unbleached nucleolar compartment, confirming that the extra-nucleolar space is a high-mobility compartment.

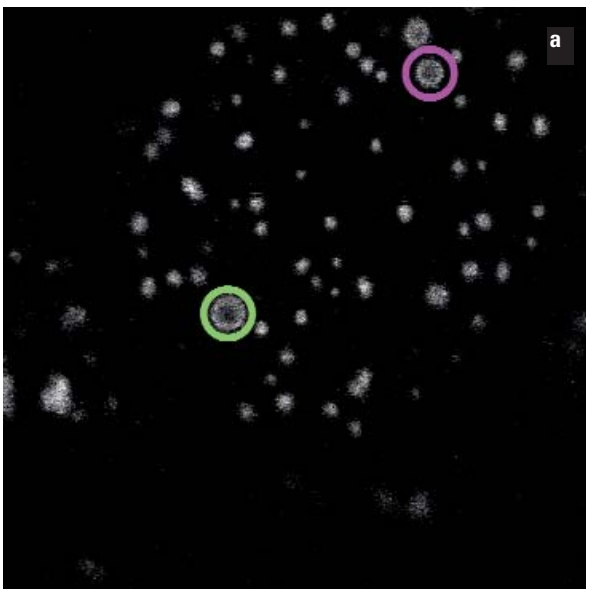

Box **4**, figure **1a**: Fluorescence Recovery After Photobleaching: application for dynamic studies of nuclear bodies I (courtesy of Dr. Massimiliano Garre', IFOM-IEO-Campus, Milano). The photolysis locally induced by intense illumination can reveal information on molecular dynamics of single compartments of the nucleus (in this case of the nuclear bodies where a fusion of GFP to the PML protein is localized).

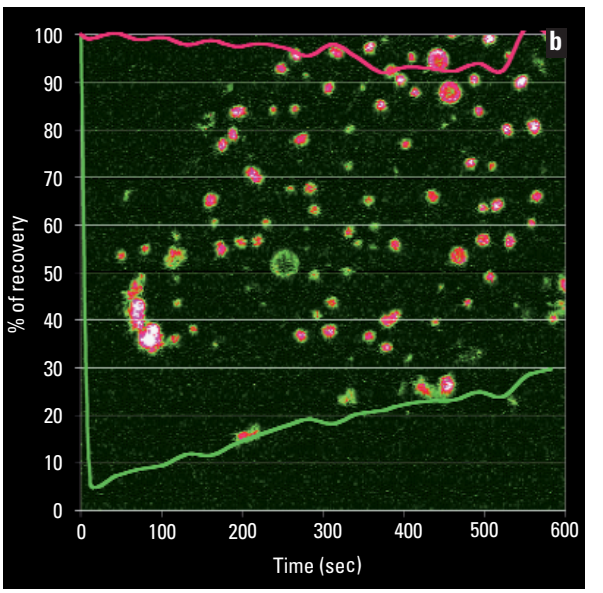

Box **4**, figure **1b**: Graphical display of how the signal recovers with time (over ca. 10 minutes), indicating potential structural features of the protein analyzed. A second structure (violet curve) does not show any recovery.

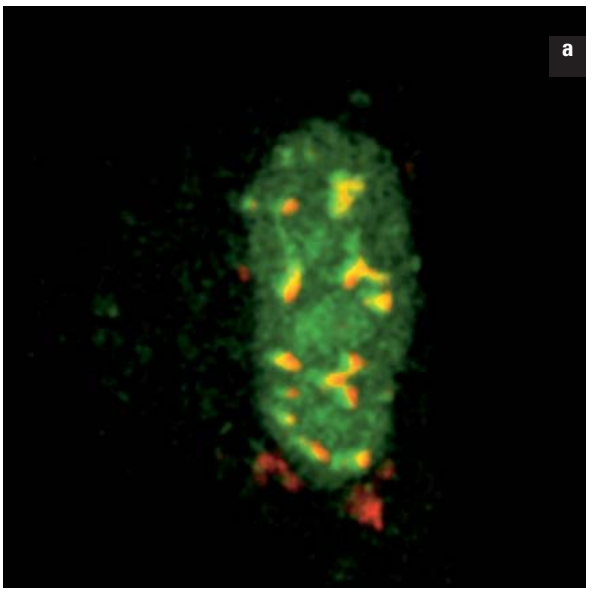

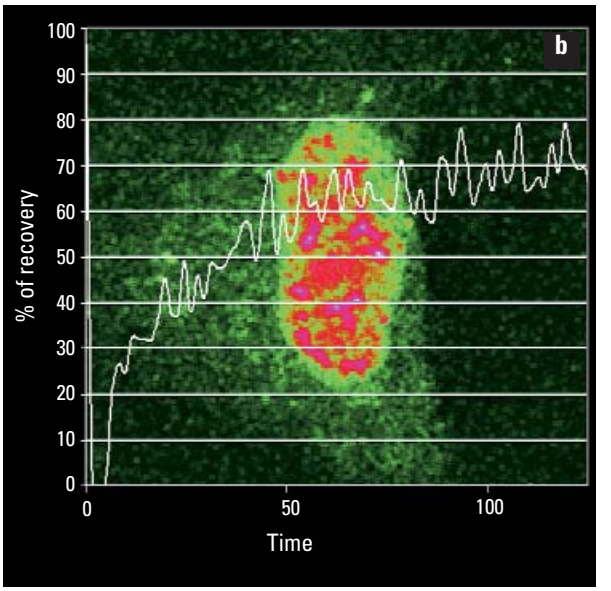

Box **4**, figures **2a, b**: Fluorescence Recovery After Photobleaching: application for studying dynamics of nuclear bodies II (courtesy of Dr. Sara Barozzi, IFOM-IEO-campus, Milano). The studies on the dynamic properties of protein p53 (GFPp53) in relation to nuclear bodies containing PML (CFPPML) show the accumulation of p53 with the structural component (PML). Figure **2a**: Indication of the colocalization of the two signals, figure **2b**: Recovery of the signal which is a result of a continuous flow of molecules from the nuclear area.

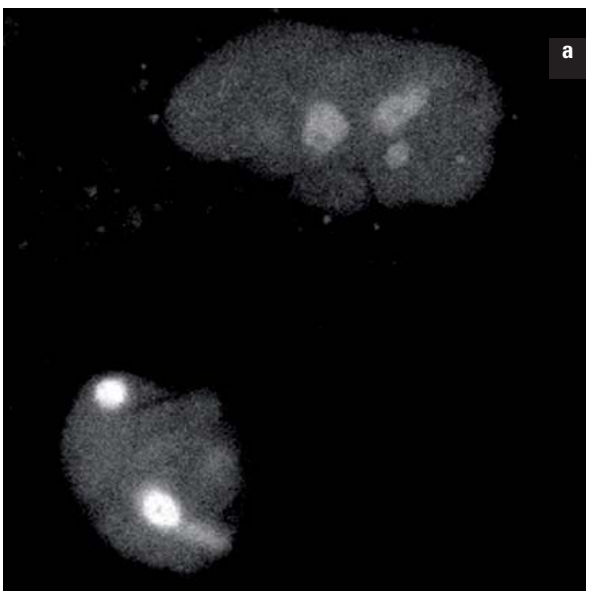

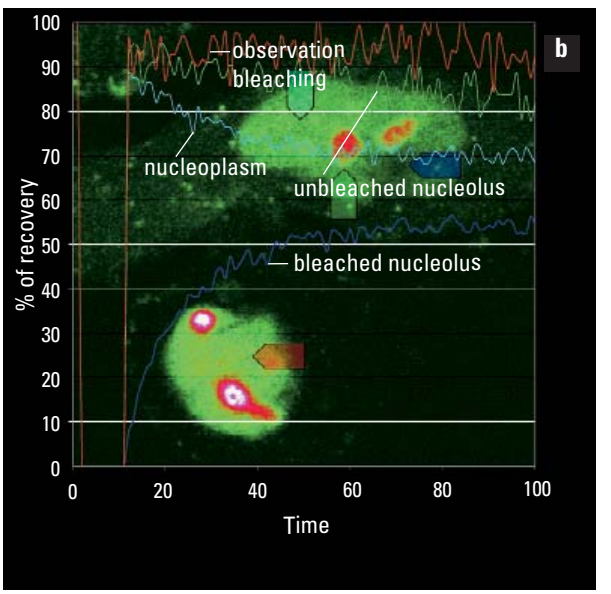

Box **4**, figures **3a, b**: Fluorescence Recovery After Photobleaching: application for studying dynamics of nuclear bodies III (courtesy Dr. Sara Barozzi, IFOM-IEO-campus, Milano). Studies of dynamic properties of the fusion protein GFP-p19. The localization of p. 19 in the nucleus (figure **3a**) is characterized by a typical dynamic. This is demonstrated by the course of fluorescence recovery (figure **3b**, blue line) after photobleaching of a nucleous. The analysis of various regions in the nucleus shows how the signal recovery stems basically from a fraction of molecules that diffuse in the nucleoplasm.

2.2 Fluorescence Resonance Energy Transfer (FRET): Nanometric Rulers (by Valentina Caorsi, LAMBS MicroscoBio, University of Genoa)

Historically, fluorescence microscopy always represented a powerful instrument for studying structure-function relations and in particular for investigating biomolecular interactions. If two fluorescence signals are colocalized in a confocal microscope, this indicates their spatial proximity below optical resolution (distances of 100 nm lateral, 300 nm axial with high-NA optics). It does not necessarily reveal information on their interaction.

A process that is based on Förster Resonance Energy Transfer (FRET) allows measurement of distances between two molecules in the range of a few nanometers. FRET is essentially a quenching effect: if a fluorescent molecule – the donor – has absorbed a photon that promoted the molecule to the first excited state, the energy may be transferred to a second molecule – the acceptor, instead of being released as fluorescence emission. This transfer occurs without any radiation. Eventually, the second fluorochrome will emit a fluorescence photon and thus decay to the ground state. In an experiment, one can consequently observe an emission at the acceptor's emission wavelengths upon excitation at the donor's absorption wavelengths.

Boundary conditions for FRET to occur efficiently are

- a large overlap of the donor emission spectrum and the acceptor absorption spectrum
- a donor-acceptor distance close to a critical value (Förster radius)
- a high donor quantum yield
- an appropriate orientation of the transition dipoles

The Förster radius is defined as the donor-acceptor distance at which FRET efficiency is 50%, i.e. half of the excited donors transfer their energy to acceptor molecules. The Förster radius depends on the fluorophore's photophysical properties and it varies in a range of distances between 1 and 10 nm. These values justify the definition of a FRET process as a nanometric ruler as it allows, once a FRET efficiency is measured, intermolecular distances to be determined on the nanometer scale. The distance measured by FRET depends on the fluorescent parts of the molecules investigated. I.e. no FRET indicates that the distance of the fluorophores which are linked to the molecule in question is larger than the Förster radius. The spatial arrangement of the biological molecules is not directly accessible. The mode of labelling biomolecules with fluorescent probes is important and it is useful to gain knowledge about the tertiary and quaternary structure that is obtained by crystallography. Much of the published work on FRET is on purified enzymes and tries to understand the fluorophore's location through conformational changes during the catalytic reaction. *In vitro* labelling of biomolecules employs specific chemical compounds based on aminic or thiolic groups that increase the degree of freedom concerning the location of the FRET couple. For *in vivo* the situation is different: fluorescent labels are typically GFPs that are fused to structural proteins or other markers. The most commonly used FRET pair for *in vivo* studies is CFP (Cyan Fluorescent Protein) and YFP (Yellow Fluorescent Protein). However, these proteins are very large and have a certain propensity to attenuate or even cancel the effect. Nevertheless, they are a powerful instrument for studying specific activities in the cell.

Other than the method of staining two different proteins to monitor interactions, it is possible to use appropriate FRET probes to follow the dynamics of chemical reactions *in vivo*. These probes have e.g. CFP and YFP coupled to a sensor that changes conformation upon binding to the appropriate ligand. The conformational shift alters the distance from donor to acceptor which in turn will cause a variation in FRET efficiency. The most famous example is probably the Cameleon sensor which is used to measure Calcium concentration (changes). Here, CFP and YFP are bound to either ends of a calmodulin molecule. In the presence of calcium ions, the calmodulin undergoes a conformational change and brings the two labels closer together. This is used as a reporter of Ca-ions in living cells. On the same principle, a sensor for GTPasic activity of RAS or for studying tyrosine-kinase activity of proteins is available. The compatibility of such probes with living conditions allows spatial and temporal tracking of intracellular processes and identification of cellular compartments that are involved in particular biological activities. Besides conformational probes, there is also a different kind of probe available that is particularly helpful in measuring ac-

tivities of enzymes like trypsin and caspase (enzymes involved in apopoptosis). The FRET efficiency of these probes is high, as long as a peptidic bridge between CFP and YFP is intact. The lytic activity can split the peptide bond and the FRET signal decreases.

The same principle is used for the *molecular beacon*, a probe for measuring metal-protease activity in extracellular matrix in live animals. The peculiarity of these probes, from a photophysical point of view, is related to the specific FRET pair used, consisting of two identical molecules of the dye Cy5. The partial spectral overlap of excitation and emission causes resonance energy transfer between identical molecules. In this particular situation, FRET is accompanied by total quenching. When the peptide bond is cleaved, the Cy5 molecules separate and start emitting fluorescence.

The great variability of applications based on FRET processes is associated with a similarly wide range of detection methods. The simplest technique detects FRET by sequentially measuring the ratio of the emitted fluorescence signals. It is extremely fast, being based on the collection of emission of the donor and acceptor upon excitation of the donor. The ratio of these two emissions will change depending on the FRET efficiency. When FRET is increased, the donor will emit less and the acceptor will increase in emission. This method is particularly helpful in monitoring extremely fast events, where the ratio trends give a clear indication of FRET increase or decrease. However, many factors can impair the validity of this approach due to the high number of artefacts, in particular if applied in static situations on fixed samples. Acceptor emission can be falsely measured by direct excitation of acceptor molecules by the donor excitation (excitation crosstalk). CFP, for example, has an excitation

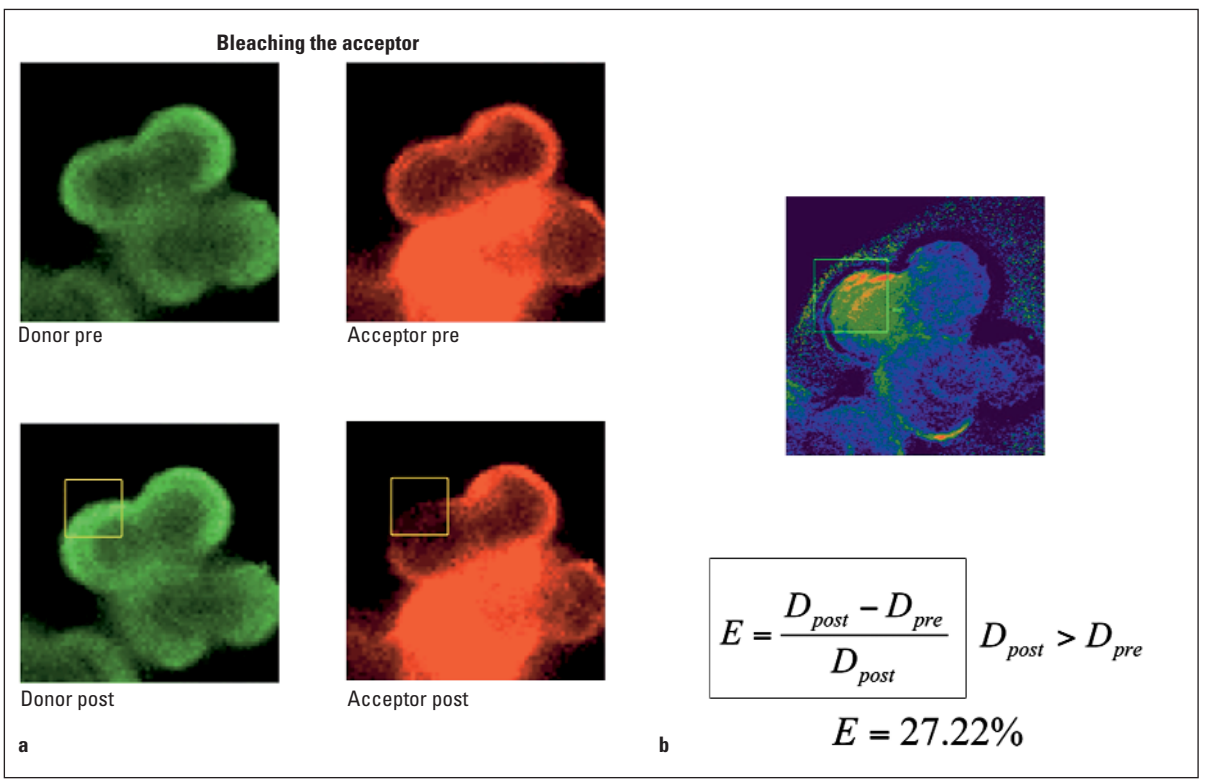

Figure **10**: Fluorescence Resonance Energy Transfer (FRET). (Courtesy of Dr. Valentina Caorsi LAMBS, microscoBio, Genova). Analysis of resonant energy transfer by acceptor photobleaching. If FRET occurs, the donor molecule is de-excited by transferring the energy without radiation to the acceptor molecule, which emits a photon in the acceptor emission band. If the acceptor molecules are destroyed, the non-radiative process cannot occur and the donor emits more light than before (figure **10a**). In figure **10b** the calculated FRET efficiency is shown as a false-colour image, according to the formula shown in the insert.

peak at ca. 430 nm, where YFP is still absorbing at ca 10% of its maximum. When the YFP is much more expressed than the CFP fusion, this may cause a very significant false FRET contribution. Increased fluorescence in the acceptor channel may also be caused by donor emission into the acceptor emission band. To compensate for these errors, protocols have been implemented, where images are acquired from samples containing either donor or acceptor only. When the spectral overlaps contribution were calculated, one can correct for the various crosstalk effects in images collected from FRET samples.

But there are still sources for errors. Let us consider a situation where we want to evaluate the area of maximum activity of a specific enzyme as mentioned above. Even if we have a unitary stoichiometric ratio of donor and acceptor molecules, spectral interference phenomena may occur. From a photophysical point of view, CFP has a really low quantum yield in comparison to the yield of YFP. Spectral consideration can help to reduce these problems to a tolerable amount. For example, donor excitation may be shifted to the blue violet range (405 nm) instead of 458 nm. And the acceptor emission may be detected in the farther red area, where donor emission is reduced.

A different method of measuring FRET is based on acceptor photobleaching. When FRET occurs, the donor emission will be decreased. Consequently, the donor emission can be restored when the acceptor molecule is destroyed. After the bleaching of the acceptor, the donor fluorescence will increase and reveals the previous FRET efficiency.

The acceptor photobleaching method is quite difficult to apply *in vivo* for studying fast dynamics, but is one of the most accepted methods for demonstrating FRET occurrence in fixed samples. FRET efficiency is calculated by the following formula:

$$E = 1 - \frac{D_{pre}}{D_{post}}$$

where Dpre and Dpost represent donor fluorescence in the presence and absence of the acceptor molecule respectively. Nevertheless, the quantification is also impaired by severe side effects due to strong illumination during the bleaching of the acceptor. It is necessary to take careful control measurements. The choice of excitation wavelength far from donor absorption can improve the FRET measurements, but this option is not always available.

The methods described above for FRET evaluation are based on intensity. Alternatively, fluorescence lifetime measurements can also be employed for these measurements and are less prone to the errors as described above. The fluorescence lifetime is the mean time the molecule spends in the excited state and ranges typically somewhere from 0.5 ns to 5 ns. If FRET occurs, the lifetime is reduced. This measurement is independent of the number of fluorescent molecules.

While the intensity-based FRET measurements can be performed with any fluorescence microscope, even non-confocal, lifetime measurements need a specific experimental setup with pulsed sources, typically with lasers used for multiphoton microscopy, and specific processing of the recorded signals.

Insert 5: Förster Resonance Energy Transfer (FRET)
(by Valentina Caorsi, LAMBS-MicroSCoBio, University of Genoa)

FRET, Förster Resonance Energy Transfer, classically refers to a physical process by which a molecule, the donor, transfers its energy to a nearby molecule, the acceptor, by means of a radiation free dipole-dipole interaction. In the case of fluorescent molecules, FRET may also refer to Fluorescence Resonance Energy Transfer.

A short donor-acceptor distance (in the range of 1-10nm) is a necessary condition for FRET to occur, but it is not sufficient. A large spectral overlap between donor emission spectrum and acceptor absorption spectrum is also essential. In addition, FRET depends on donor quantum yield and mutual donor and acceptor orientation.

For a donor molecule D in a distance r to an acceptor molecule A, we can assume each molecule as a dipole oscillating at a certain frequency. When the distance is short enough, the transition dipoles can enter a resonance condition. The rate K_T of energy transferred from D to A is related to the donor-acceptor distance as follows:

$$k_T = \frac{1}{\tau_D}\left(\frac{R_0}{r}\right)^6$$

where τ_D is the donor lifetime in the absence of the acceptor and R_0 is the Förster radius, the distance at which FRET efficiency is 50%. The FRET efficiency E is the fraction of photons absorbed by the donor that are transferred to an acceptor. It can be calculated as the ratio of the transfer rate K_T to the total decay rate of the donor, which is the sum of transfer and fluorescence:

$$E = \frac{k_T}{k_T + \frac{1}{\tau_D}}$$

Substituting expression given above for K_T, we obtain:

$$E = \frac{1}{1 + \left(\frac{r}{R_0}\right)}$$

Since E depends on the inverse of the sixth power of the donor-acceptor distance r, the range in which FRET occurs is limited to a narrow band, typically in the range of 1...10 nm. Consequently, a FRET signal in a particular location in the acquired image gives further spatial information that is more accurate than the optical resolution of the microscope (~200 nm). In summary, the conditions for efficient FRET measurements are:

1. donor and acceptor distance 1...10 nm
2. spectral overlap of donor emission and acceptor absorption ≥ 30%
3. donor and acceptor transition dipoles sufficiently aligned

If, in a FRET experiment, the acceptor molecules get closer to the donor molecules, the donor fluorescence decreases, whereas – due to the energy transfer – the acceptor fluorescence increases simultaneously. FRET efficiency is simply the ratio of donor fluorescence intensities in the presence (I_{DA}) and in the absence (I_D) of the acceptor:

$$E = 1 - \frac{I_{DA}}{I_D}$$

The energy transfer from donor to acceptor is a competitive pathway for excited molecules to decay to the ground state. Consequently, the ratio of donor lifetime in the presence τ_{DA} and in the absence τ_D of the acceptor can also be used to calculate FRET efficiency:

$$E = 1 - \frac{\tau_{DA}}{\tau_D}$$

Another way of determining FRET efficiency is to compare donor fluorescence intensity before and after the complete photodestruction (photobleaching) of the acceptor: if all acceptor molecules are destroyed by photobleaching, donor molecules cannot release energy to the acceptor. Consequently, the donor fluorescence intensity is increased. E is quantified by calculating donor fluorescence intensity before ($I_{DA,\,pre}$) against after the complete photobleaching ($I_{DA,\,post}$) of the acceptor:

$$E = 1 - \frac{I_{DA,\,pre}}{I_{DA,\,post}}$$

From the measured FRET efficiency, the distance r between the donor and acceptor can be obtained if the Förster radius R_0 is known:

$$r = R_0 \left(\frac{1}{E} - 1 \right)^{\frac{1}{6}}$$

As mentioned, a necessary condition for FRET to occur is a sufficient spectral overlap. This causes the problem of channel crosstalk and makes interpretation of FRET images quite difficult. Two types of problem have to be considered: Spectral-Bleed-Through (SBT) and crosstalk.

Particular examples of SBT are:

1. ASBT (Acceptor Spectral-Bleed-Through): acceptor molecules are directly excited by the donor absorption wavelength;
2. DSBT (Donor Spectral-Bleed-Through): donor molecules directly emit in the acceptor channel.

For crosstalk we have:

1. donor molecules which are directly excited by the acceptor absorption wavelength;
2. acceptor molecules which directly emit in the donor channel.

Many methods are published that try to overcome these problems. Most of them are based on sensitized emission measurements trying to correct fluorescence intensities by introducing other information such as sample characteristics and dye concentrations. Others try to use ratiometric analysis in the hypothesis that SBT is independent of fluorophore intensity, other SBT and crosstalk levels are determined at different fluorescence intensities. An improvement will certainly come by the utilization of white light laser sources allowing to select the optimal excitation wavelengths and to realize a sort of *optimized excitation selection* increasing the distance between the donor and acceptor useful lines.

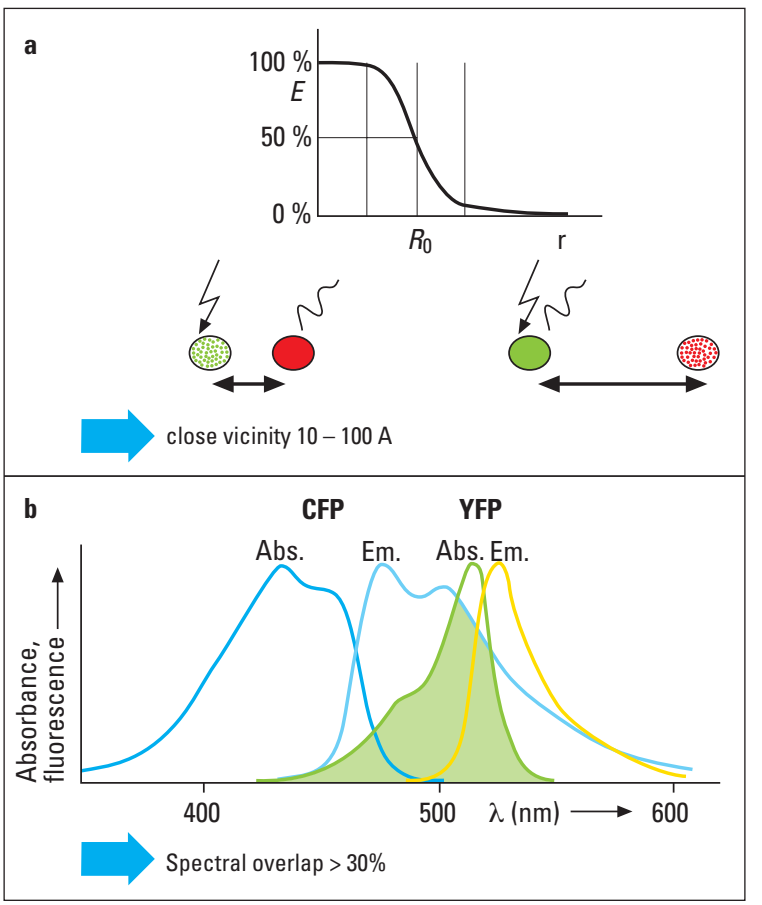

Box **5**, figure **1**: Förster Resonance Energy Transfer: The transfer of energy without radiation, the base of the FRET phenomenon, requires a spatial distance of less than 10 nm between donor and acceptor molecules. The dependence of FRET on the distance is shown in figure **1a**. A second condition for FRET to occur is the overlap of emission spectrum of the donor and excitation spectrum of the acceptor. Figure **1b** shows this spectral overlap for the FRET pair CFP and YFP, which is commonly used for FRET experiments (p. 34).

3

3. The Two-Photon (2P) Revolution: from Heisenberg to Feynman. Realizing Ideas, Making Dreams Come True

3.1 Introduction

Here we move towards the domain of two-photon excitation microscopy where Heisenberg meets Feynman in a race to surpass limitations of *conventional* optical microscopy using new technologies for old and brilliant ideas. A revolution in microscopy that started more than 70 years ago and that is drawing our attention to a multidimensional way of interpreting signals and analysing data. From the conquest of the third dimension to the seventh, attempting to overcome the optical resolution barrier. A sort of paradox when using twice the wavelength normally used and without violating Abbe's law. It has already been demonstrated that some time, dreams will become reality.

3.2. Brief Historical Background

Two-photon excitation microscopy has its roots in two-photon absorption, which dates back more than 70 years. In 1931, Maria Göppert-Mayer published her brilliant doctoral dissertation on the theory of two-photon quantum transitions in atoms and established the theoretical basis of two-photon excitation. The two-photon excitation process can take place if two low energy photons are able to interact simultaneously with the very same fluorophores. Here, the time scale for *simultaneous interaction* is the time scale of molecular energy scales. Using the Heisenberg uncertainty principle and probability considerations, we arrive at a very small number, i.e. $10^{-16} - 10^{-15}$ s. This time scale gives an idea of the rarity of the event and the difficulty of its implementation. The two-photon excitation effect predicted by Maria Göppert-Mayer was not experienced until in the 60 s, after the development of a very insensitive light source as the laser. In 1961 Kasier and Garret observed two-photon excitation fluorescence of $CaF_2:Eu^{2+}$. In 1964, Sigh and Bradley were able to evaluate the three-photon absorption cross-section of naphthalene crystal. In 1970 Rentzepis and co-workers observed a three-photon excitation of organic dye. Other non-linear related effects as second-harmonic generation were observed in the 60 s and 70 s: in 1974 Helvet and Christen recorded at the microscope level a second-harmonic signal generated by ZnSe polycrystal; this result confirms the previous experiments made by Franken and co-workers in 1961. In 1976 Berns reported a probable two-photon effect as a result of focusing an intense pulsed laser beam onto chromosomes of living cells, and such observations form the basis of modern nano-surgery, nowadays developed by Karsten König. We have to wait until 1978 to find the description of the first nonlinear scanning optical microscope with depth resolution and 3D capabilities. The first three-dimensional non-linear excitation microscopy image was obtained by the Oxford group, composed by Sheppard, Kompfner, Gannaway and Choudury, the same group that with the help of Wilson developed the modern confocal microscope in the UK. Sheppard and co-workers showed how the high localization of the non-linear excitation obtained in the focus region is an optimal feature for optical sectioning. Further, they demonstrated experimentally the occurrence of two-photon excitation, showing the square dependence between intensity emission and excitation average power, and outlined a possible application in fluorescence microscopy. Unfortunately, the intense energies required did not allow scientists to effectively study biological systems at that time. Not until the beginning of the 1990s were the first effective and successful applications of two-photon excitation to fluorescence microscopy of biological systems reported by Winfried Denk and colleagues, under the supervision of Watt. W. Webb. They demonstrated that images could be obtained with excellent optical sectioning ability while preserving cell integrity and viability. The demonstration of the use of two-photon excitation (2PE) for optical section imaging of living biological systems started a new revolution which led to a growth of two-photon excitation scanning microscopy. The very trigger for a fast uptake of 2PE microscopy in biology was the development of commercially available mode-locked lasers, with high peak-power femtosecond pulses and repeti-

tion rates around 100 MHz. These lasers are able to preserve two of the most important requirements of two-photon excitation microscopy, namely: high density of photons in the focus region to increase the probability of the two-photon excitation events, because they are very rare at ordinary light intensity; reduction of the damage and low perturbation of the sample. A very large amount of intensity is used (order of GW/cm^2) in a very short temporal window (order of femtosecond) which allows tolerable average energies to be delivered to the samples.

Recently, another very important contribution to the success of 2PE microscopy is the continuous development of new imaging strategies such as STED and 4PI by Stefan Hell, who crossed a new frontier in microscopy with the aim of switching from microscopy to nanoscopy. This switching is consolidated by the introduction of techniques like PALM by Eric Betzig and STORM by Xiaowei Zhuang. We can state that a new revolution is on the way.

3.3 Two-Photon "Rendezvous"

3.3.1 Transferring Energy by (not Exactly Comfortable) Instalments

In 2PE of fluorescence, two low energy photons – emitted at a wavelength that is more or less twice the one needed to prime fluorescence in a conventional way – are involved in the interaction with absorbing fluorescent molecules. The excitation process can take place if these two low energy photons are able to interact simultaneously with the very same fluorophore within a temporal window of 10^{-16} – 10^{-15} s.

These two photons do not necessarily have to be identical but the sum of their respective wavelengths have to fill the energetic gap allowing to prime fluorescence emission as in a conventional one-photon absorption process. This situation, compared to the conventional one-photon excitation process, is shown in figure **11** using a Perrin-Jablonski-like diagram where the possible existence of a virtual state is sketched. It is worth noting that for practical reasons the experimental choice is usually such that such wavelengths are identical. So in a 2PE process it is crucial to combine sharp spatial focusing with temporal confinement of the excitation beam.The process can be extended to n-photons requiring higher photon densities temporally and spatially confined, see figure **12**. Thus, near infrared (680 – 100 nm circa) photons can be used to excite UV and visible electronic transitions producing fluorescence. The typical photon flux densities are of the order of more than 10^{24} photons cm^{-2} s^{-1}, which results in light intensities around MW-TW cm^{-2}.

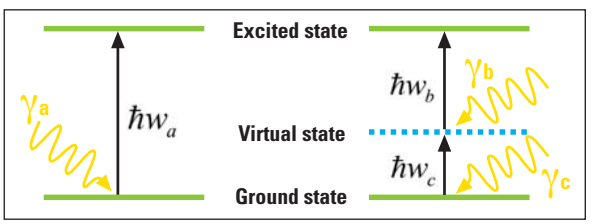

Figure **11**: Illustration by a simplified Perrin-Jablonski diagram of the excitation process by two photons (right) in comparison to the *conventional* excitation process (left). The process of excitation with two photons requires two photons to be involved simultaneously that carry together the same energy that would conventionally be needed to move the molecule into the excited state.

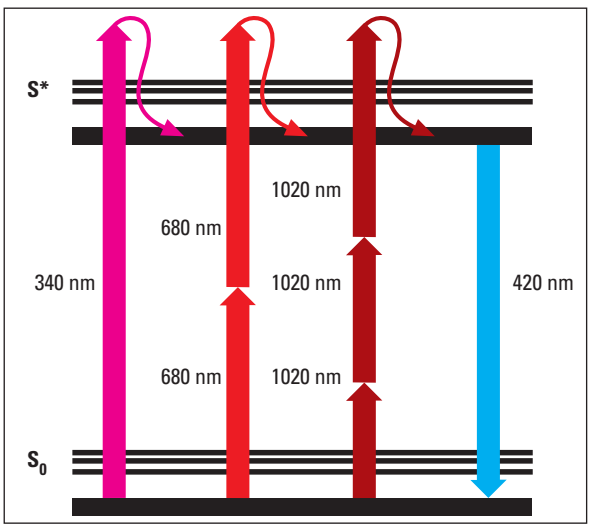

Figure **12**: Illustration of excitation processes with one, two or more photons. In this case, a molecule which requires excitation at 340 nm is possibly excited by a multiphoton process, where the energy is delivered in portions. For example, the molecule can be excited by a two-photon process by irradiation with a wavelength of 680 nm (1020 nm with three-photons, and so on). The emission that follows the excitation by the various described processes is always identical, as far as the spectral parameters are concerned.

Since the simultaneous absorption of two photons can be treated as the advent of two independent events, each of them related to the emission of fluorescence intensity, 2PE is a process that has a quadratic dependence on the instantaneous intensity of the excitation beam. Introducing the two-photon molecular cross section as the propensity of the fluorescent molecule to absorb in a 2PE process photons having a certain energy or wavelength, and referring to the fluorescence emission as a function of the temporal characteristics of the light, $I_f(t)$, to it, one has:

$$I_f(t) \propto \delta_2 * I(t)^2 \propto \delta_2 * P(t)^2 \left(\pi \frac{(NA)^2}{hc\lambda} \right)^2$$

where $I_f(t)$ is the fluorescence intensity per molecule, $\delta_2(\lambda)$ the two-photon molecular cross section, P(t) the laser power, and (NA) the numerical aperture of the focusing objective lens. The last term of the previous equation simply takes care of the distribution in time and space of the photons by using paraxial approximation in an ideal optical system. Now, for a pulsed laser beam with pulse width, τ_p, repetition rate, f_p, and average power

$$P_{ave} = D * P_{peak}(t)$$

where $D = \tau_p * f_p$, the approximated P(t) profile can be described as

$$P(t) = P_{ave} / D \qquad \text{for } 0 < t < \tau_p$$

$$P(t) = 0 \qquad \text{for } \tau_p < t < (1/f_p)$$

one has:

$$< I_{f,p}(t) > \propto \delta_2 \frac{P_{ave}^2}{\tau_p^2 f_P^2} \left(\pi \frac{(NA)^2}{hc\lambda} \right)^2 \frac{1}{T} \int_0^{\tau_p} dt = \delta_2 \frac{P_{ave}^2}{\tau_p f_P} \left(\pi \frac{(NA)^2}{hc\lambda} \right)^2$$

It is possible to demonstrate that, in comparison with CW lasers, pulsed lasers operate at the very same excitation efficiency, i.e. fluorescence intensity per molecule, of CW lasers delivering an average power higher than the one needed by a pulsed laser of a factor $(\tau_p \cdot f_p)^{-1/2}$. The most popular relationship reported by Winfried Denk in 1990 is related to the probability, n_a, that a certain fluorophore simultaneously absorbs two photons during a single pulse, again in the paraxial approximation one has:

$$n_a \propto \frac{\delta_2 \cdot P_{ave}^2 \cdot}{\tau_p f_p^2} \left(\frac{NA^2}{2hc\lambda} \right)^2$$

Introducing 1 GM (Göppert-Mayer) = 10^{-58} [$m^4 \cdot s$], for a δ_2 of approximately 10 GM per photon, focusing through an objective of NA >1, an average incident laser power of $\approx 1^{-50}$ mW, operating at a wavelength ranging from 680 to 1100 nm with 80 – 150 fs pulse-width and 80 – 100 MHz repetition rate, would saturate the fluorescence output as for one-photon excitation. This suggests that for optimal fluorescence generation, the desirable repetition time of pulses should be in the order of a typical excited-state lifetime, which is a few nanoseconds for commonly used fluorescent molecules. For this reason the typical repetition rate is around 100 MHz. Now, one can estimate n_a for a common fluorescent molecule like fluorescein, that possesses a two-photon cross-section of 38 GM at 780 nm, saturation starts occurring at an average excitation power of 10 mW. The related rate of photon emission per molecule, at a non saturation excitation level, in the absence of photobleaching is given by n_a multiplied by the repetition rate of the pulses. This means approximately $5 \cdot 10^7$ photons s^{-1}. It is worth noting that when considering the effective fluorescence emission one should consider a further factor given by the so-called quantum efficiency of the fluorescent molecules. It has also been demonstrated that the fluorophore emission spectrum is independent of the excitation mode. Tables **3.3.1a** and **3.3.1b**, p. 40 report the optimal wavelengths for exciting within the 2PE regime fluorescent molecules, including autofluorescent ones. Now, even if the quantum-mechanical selection rules for 2PE differ from those for one-photon excitation, several common fluorescent molecules can be used. Unfortunately, the knowledge of one-photon cross section for a specific fluorescent molecule does not allow any quantitative prediction of the 2P trend. The only "rule of thumb" that one could use is related to the possibility of having an effective 2PE cross-section peak at double the wavelength needed for one-photon excitation. However, the cross section parameter is now available for a wide range of dyes including quantum dots.

Table **3.3.1a**

Extrinsic Fluorophores	λ(nm)	$\eta\delta_2$	δ_2
Bis-MSB	691/700	6.0 ±1.8	6.3 ±1.8
Bodypy	920	17 ± 4.9	–
Calcium Green	740 – 990	–	~ 80
Calcofluor	780/820	–	–
Cascade blue	750 – 800	2.1 ± 0.6	~ 3
Coumarin 307	776, 700 – 800	19 ± 5.5	~ 20
CY2	780/800	–	–
CY3	780	–	–
CY5	780/820	–	–
DAPI (free)	700/720	0.16 ± 0.05	~ 3.5*
Dansyl	700	1	–
Dansyl Hydrazine	700	0.72 ± 0.2	–
Dil	700	95 ± 28	–
Filipin	720	–	–
FITC	740 – 820	–	~ 20 – 38*
Fluorescein (pH ~ 11)	780	–	38 ± 9.7
Fura-2 (free)	700	11	–
Fura-2 (high Ca)	700	12	–
Hoechst	780/820	–	–
Indo-1 (free)	700	4.5 ± 1.3	12 ± 4
Indo-1 (high Ca)	590/700	1.2 ± 0.4	2.1 ± 0.6
Lucifer Yellow	840 – 860	0.95 ± 0.3	~ 2
Nile Red	810	–	–
Oregon Green Bapta 1	800	–	–
Rhodamine B	840	–	210 ± 55
Rhodamine 123	780 – 860	–	–
Syto 13	810	–	–
Texas red	780	–	–
Triple probe (Dapi, FITC, and Rhodamine)	720/740	–	–
TRITC (rhodamine)	800 – 840	–	–

Table **3.3.1b**

Intrinsic Emitters	λ(nm)	δ_2
GFP wt	800 – 850	~ 6
GFP S65T	~ 960	~ 7
BFP	780/820	–
CFP	780/840	–
YFP	860/900	
EGFP	940 – 1000	~ 250
DsRed-Coral Red	960 – 990	~ 20 – 110
Citrine- Coral yellow	950	~ 70
Phycoerythrin	1064	~ 300
Flavins	~ 700 –730	~ 0.1 – 0.8
NADH	690 – 730	~ 0.02 – 0.09
Retinol	700 – 830	~ 0.07
Pyridoxine	690 – 710	~ 0.008
Folic acid	700 –770	~ 0.007
Lipofuscin	700 – 850	–
Collagen, Elastin	700 – 740	–
Qdts	700 – 1000	~ 2000 – 47000

3.3.2 Spatial Localization of Two-Photon Events

In optical terms, the two-photon effect has the important consequence of limiting the excitation region within a sub-femtoliter volume. This 3D confinement of the two-photon excitation volume can be understood on the basis of optical diffraction theory. Using excitation light with wavelength λ, the intensity distribution at the focal region of an objective with numerical aperture $NA = \sin(\alpha)$ is described, in the paraxial regime, by:

$$I(u,v) = \left| 2\int_0^1 J_0(v\rho) e^{-\frac{i}{2}u\rho^2} \rho \, d\rho \right|^2$$

where J_0 is the zero order Bessel function, ρ is a radial coordinate in the pupil plane,

$$u = \frac{8\pi \sin^2(\alpha/2) z}{\lambda} \quad \text{and} \quad v = \frac{2\pi \sin(\alpha) r}{\lambda}$$

are dimensionless axial and radial coordinates, respectively, normalized to the wavelength. Now, the intensity of fluorescence distribution within the focal region has a I(u,v) behaviour for the one-photon case and for 2PE. The arguments of $I^2(u/2, v/2)$ take into proper account the fact that in the latter case one utilizes wavelengths that are approximately twice the ones used for one photon excitation. As compared with the one-photon case, 2PE intensity distribution is axially confined. In fact, considering the integral over ν, keeping u constant, its behaviour is constant along z for one-photon and has a half-bell shape for 2PE. This behaviour is responsible for the three-dimensional sharp localization of 2PE. Now, the most interesting aspect is that the excitation power falls off as the square of the distance from the lens focal point, within the approximation of a conical illumination geometry. In practice this means that due to the quadratic relationship between the excitation power and the fluorescence intensity, 2PE falls off as the fourth power of distance from the focal point of the objective. This implies that those regions away from the focal volume of the objective lens, directly related to the numerical aperture of the objective itself, do not suffer photobleaching or phototoxicity effects and do not contribute to the signal detected when a 2PE scheme is used. Because they are simply not involved in the excitation process, a confocal-like effect is obtained without the necessity of a confocal pinhole, as sketched in figure **13a**. Here, it clearly appears that an optical sectioning effect is obtained in this case, too. 2PE microscopy is intrinsically three-dimensional. It is worth noting that the optical sectioning effect is obtained in a very different way with respect to the confocal solution, see figure **14**. A very important consequence is that no fluorescence has to be wasted by removal from the detection pathway. In the 2PE case one should simply collect as much fluorescence as possible. In fact, fluorescence can come only and exclusively from the small focal volume shown in figure **13** (**a** and **b**) that is of the order of fraction of a femtoliter capacity. This implies a reduction in background with consequent increase of the signal-to-noise ratio that compensates the reduction in spatial resolution due to the wavelength being used with respect to the conventional linear excitation case, see again figure **12**. The utilization of an infrared wavelength instead of UV-visible ones also allows deeper penetration than in conventional cases, mainly due to the decrease of scattering during the excitation process. This implies that deeper targets within a thick sample can be reached, even if some other aspects have to be carefully considered. It is of great interest that the scattered emitted light can be completely collected by the photodetectors since it is exclusively originated from the 2PE volume. As depicted in figure **15**, we are in the high photon density domain requiring old (lenses) and new (pulsed lasers) devices to achieve fluorescent molecule excitation using low energy wavelengths. Figure **16** shows a very charming and interesting property related to 2PE excitation: the possibility of exciting different fluorescent molecules using a single red wavelength. This immediately reminds us that it is mandatory to have a very efficient and precise spectral detection system for producing unambiguous images.

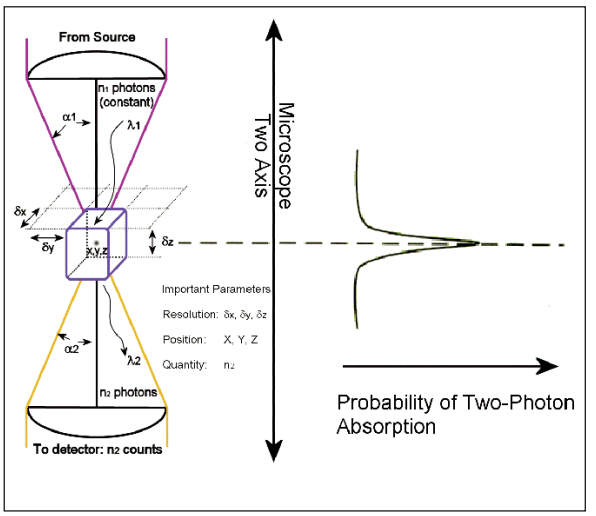

Figure **13a**

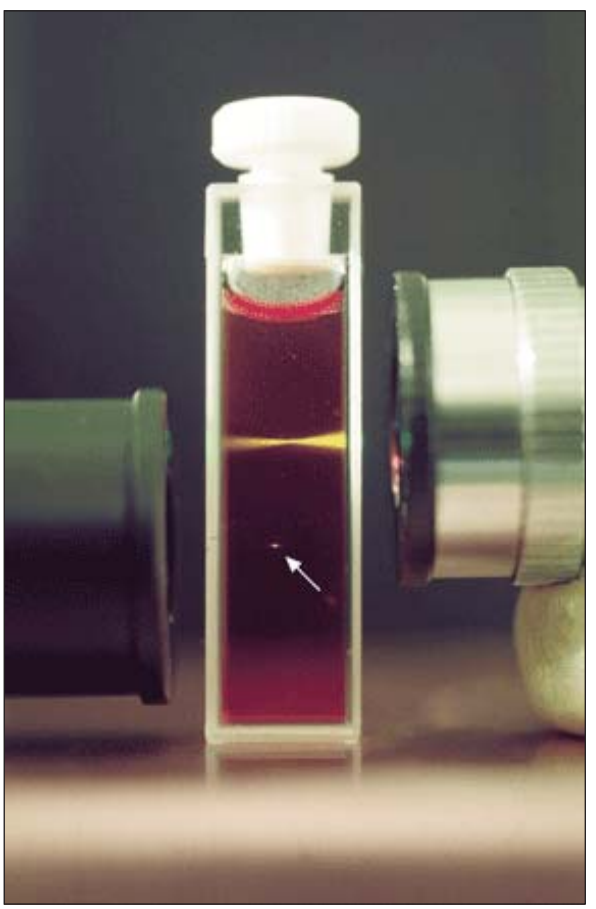

Figure **13b**

Figure **13**: This figure shows different aspects of the three-dimensional optical confinement that are characteristic for two-photon excitation. (**a**) The so-called event volume or excitation volume that results in a confined spatial region where an increased spatial and temporal concentration of photons occurs. That region coincides with the geometrical focal point of the lens and the three dimensions that can be calculated. Approximately, one can calculate a parallelepiped that is centred to the focal point and has the size of the optical resolutions in the three axes x-y-z. (**b**) Comparison of a conventional excitation process – the double cone of emission on top – and a two-photon process – the point-shaped glow at the bottom – shows how the nonlinear case creates an intrinsic 3D selection. In the conventional case it is necessary to calculate by deconvolution algorithms (computational sectioning) or by a *pinhole* (confocal scheme), in order to eliminate the extrafocal fluorescence contributions. In case of excitation by two or more photons, fluorescence occurs only in the focal point of the lens (courtesy of B. Amos, MRC, UK). (**c**) The spatial selectivity of the interaction process with two photons can also be used to create images by activation processes. The figure shows a particular photodecomposition process, or photobleaching. The upper images show the effect of photobleaching by single photon excitation in xy (left side) and in xz (right side). The two lower images show the same situation, realized by two photon excitation.

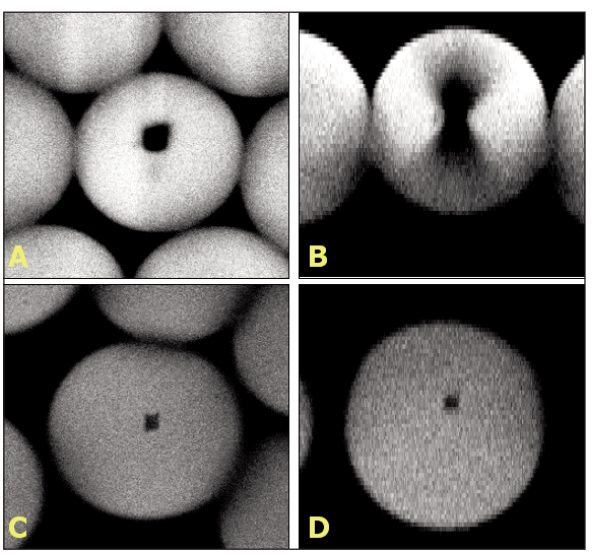

Figure **13c**

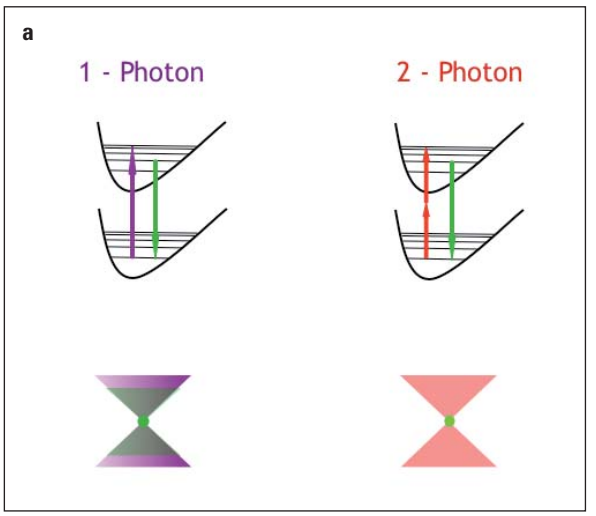

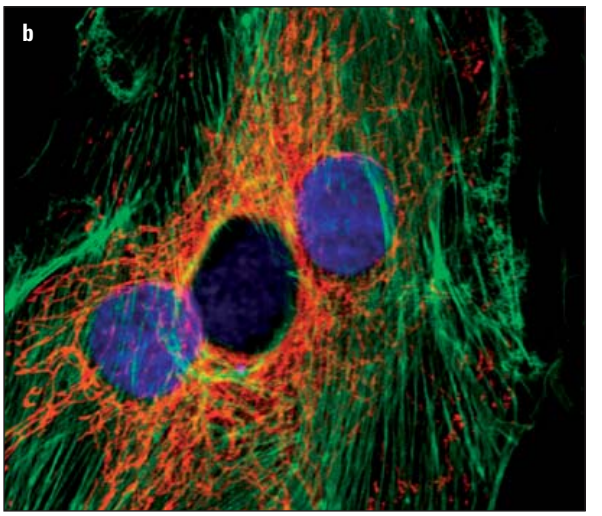

Figure **14**: (**a)** This figure illustrates the conceptual difference of 3D localization between conventional (left) and two-photon (right) excitation in analogy to the image shown in figure **13b** (courtesy of Enrico Gratton). (**b**) Demonstration of the concept by a multichannel image. Triple stained cell with fluorescences in the cell nucleus (DAPI, blue colour), where no other fluorescence adjacent to the nucleus is visible.

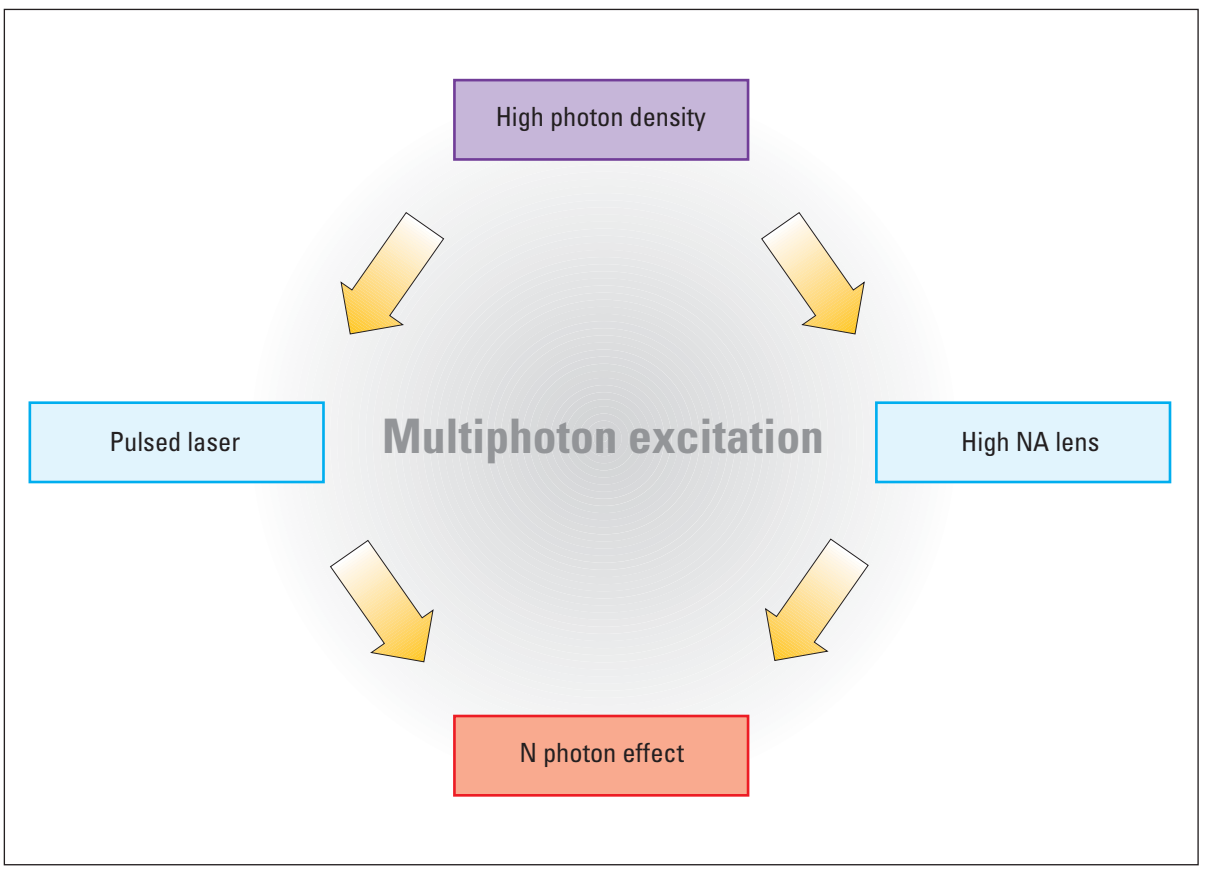

Figure **15**: To understand two-photon excitation one has to understand the excitation schemes at high photon density. It is necessary to use high-NA lenses and laser sources that allow interaction with the fluorescence molecules at increased peak power which is still tolerable in biological systems. This is possible with laser sources that emit at medium power but concentrated in short pulses of 100fs – 1ps.

Table **3.3.2**

Material Laser	Ditta; Modello	Intervallo/nm	Impulso	Frequenza	Potenza
Ti: Sapphire	Coherent; Mira	700 – 980	< 200 fs	76 MHz	0.7 W 1.3 W
	Spectra Physics; Tsunami	700 – 1000	< 100 fs (or 2 ps as option)	80 MHz	0.8 W 1.4 W
	Coherent; Chameleon – XR	705 – 980	< 140 fs	90 MHz	1.7 W
	Spectra Physics; Mai Tai	710 – 990	120 fs	80 MHz	1.5 W
	Time Bandwidth Pallas	780 – 860	< 100 fs	75 MHz	500 mW
	Time Bandwidth; Tiger	780 – 860	< 100 fs	100 MHz	400 mW
	Femtosource	750 – 850	< 12 fs	75 MHz	400 mW 600 mWF
Nd: YLF	MicroLase/Coherent Scotland; BioLite	1047	200 fs	120 MHz	500 mW
Nd: Glass	Time Bandwidth; GLX200	1058	< 250 fs	100 MHz	> 400 mW
Ytterbium	Amplitude Systems	1030	< 200 fs	50 MHz	1 W
Cr: LiSAF	Highqlasers	850 nm	100 fs	50 MHz	> 1 mW
OPO	Coherent and Spectra Physics	350 – 1200	100 fs		~ 200 mW

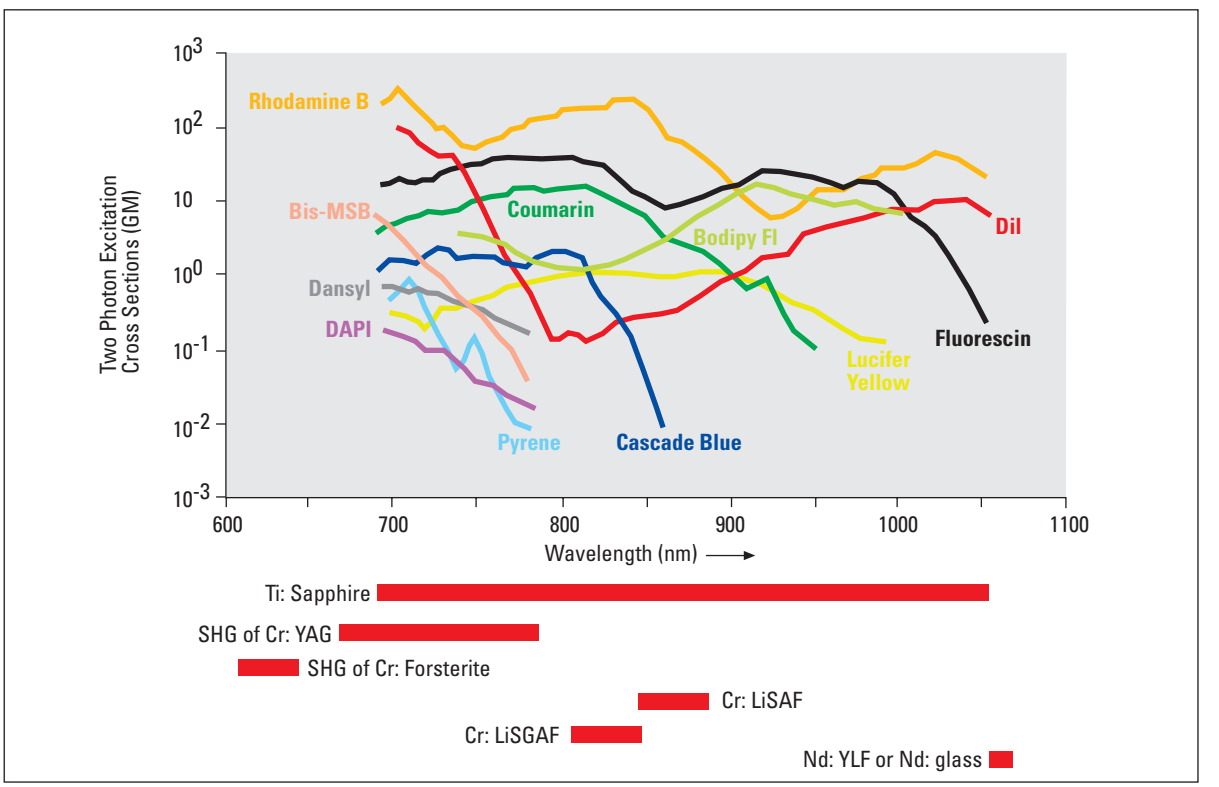

Figure **16**: Cross section relationship on wavelength for some common fluorescence molecules under two- photon excitation. The red bars at the bottom show the coverage offered by various types of laser sources.

3.4 Realizing a Multiphoton Microscope by Adapting a Confocal One

The main elements for realizing a 2PE/MPE architecture, including confocal modality, are the following: high peak-power laser delivering moderate average power (fs or ps pulsed at a relatively high repetition rate of the order of magnitude of 100 MHz) emitting infrared or near infrared wavelengths (650 – 1100 nm), laser sources for confocal 1PE, a laser beam scanning system, high numerical aperture objectives (>1), a high-throughput microscope pathway, a spectral separation module for the emitted signal discrimination, and a high-sensitivity detection system. Figure **17** sketches a general optical scheme for an MPE microscope architecture, also illustrating two popular approaches that can be used for image formation, namely: de-scanned and non de-scanned mode. The former uses the same optical pathway and mechanism employed in confocal laser scanning microscopy. The latter mainly optimizes the optical pathway by minimizing the number of optical elements encountered on the way from the sample to detectors, and increases the detector area. MPE non de-scanned mode allows very good performance given superior signal-to-noise ratio inside strongly scattering samples. In the de-scanned approach pinholes are removed or set to their maximum aperture and the emission signal is captured using the same optical scanning pathway used for excitation. In the latter, the aim is to optimize the collection efficiency: pinholes are removed and the radiation emitted without passing through the laser beam scanning mirrors. Photomultiplier tubes are the most popular detectors in MPE microscopy. Avalanche photodiodes are also excellent in terms of sensitivity, exhibiting quantum efficiency close to 70% – 80% in the visible spectral range.

CCD cameras are generally used in video rate multifocal imaging. Laser sources represent the core element for the 2PE/MPE microscope since for MPE high photon flux densities are required, > 10^{24} photons cm^{-2} s^{-1}. Using radiation in the spectral range of 650 – 1100 nm for MPE, excitation intensities in the MW-GW cm^{-2} are usually generated. Nowadays, laser sources suitable for 2PE can be described as *turnkey*

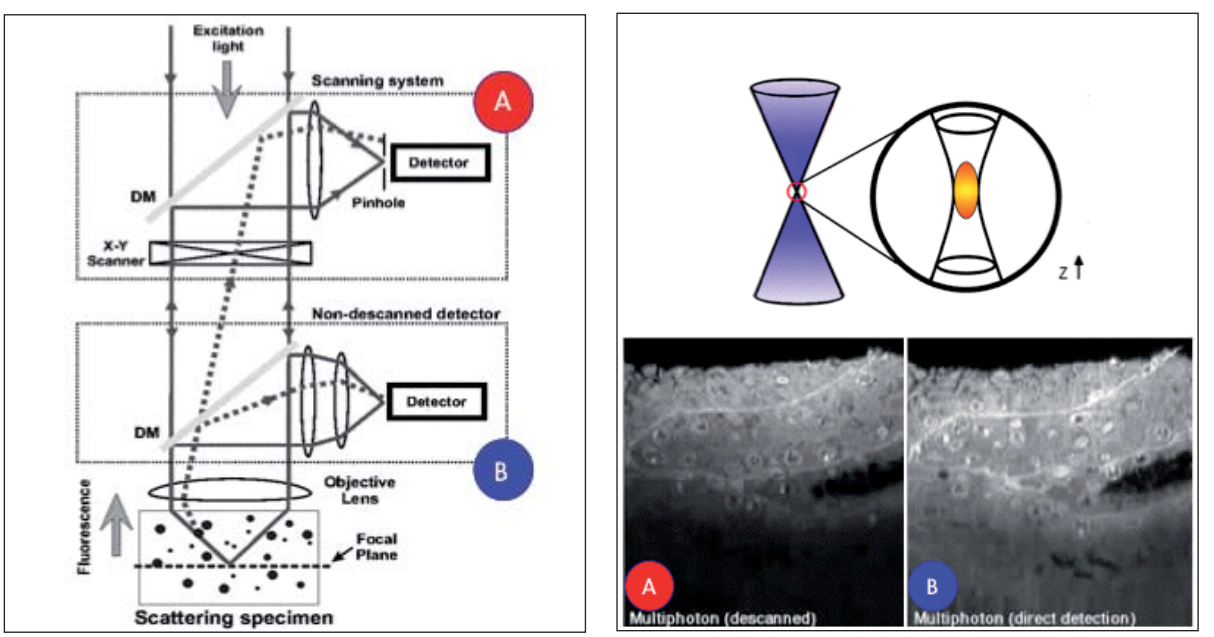

Figure **17**: Excitation scheme and acquisition in a laser scanning system. The laser light that comes from the source is directed to the actuators (scanners). It passes the objective lens and reaches the field where fluorescence is emitted. The emitted light passes the mirrors again, in order to keep the beam still. It is then directed to the pinhole, which removes the light which does not come from the focal point. In two-photon microscopy, fluorescence is only excited in the event volume. Therefore, the optical sectioning does not require a pinhole and the light can be detected without passing the scanning mirrors again. This method is called *non-descanned*. The non-descanned mode provides the possibility to collect more photons. A comparison is shown in images A (passing the scanning mirrors on the way to the detector) and B (non-descanning mode).

systems, and Ti:Sapphire lasers are the most utilized due to the high coincidence with the 2PE wavelengths needed for the majority of commonly used fluorescent molecules. Other laser sources used for 2PE are Cr-LiSAF, pulse-compressed Nd- YLF in the femtosecond regime, and mode-locked Nd-YAG and picosecond Ti:Sapphire lasers in the picosecond regime. Moreover, the absorption coefficients of most biological samples, cells and tissues are minimized within this spectral window. Table **3.3.2** reports data on some of the currently available laser sources for applications in MPE microscopy and spectroscopy. The parameters that are more relevant in the selection of the laser source are average power, pulse width and repetition rate, and wavelength range. The most popular features for an infrared pulsed laser are 700 mW^{-1} average power, 80 – 100 MHz repetition rate, and 100 – 150 fs pulse width. So far, the use of short pulses and high repetition rates is mandatory to allow image acquisition in a reasonable time while using power levels that are biologically tolerable. In order to minimize pulse width dispersion problems, operating with pulses around 150 nm should be considered. This constitutes a very good compromise both for pulse stretching and sample viability. In fact, one should remember that a shorter pulse broadens more than a longer one. Advances in laser sources are considering more compact sources, large tunability range, high average power, and special designs for tailored needs at lower prices. Objectivelenses influence the performances of any optical microscope, and for an MPE system special consideration has to be given to the numerical aperture. Moreover, adequate transmission in the IR regime has to be coupled with good collection efficiency towards the ultraviolet region.

Figure **18**: Two photon system setup on a confocal microscope at LAMBS-MicroScoBio in the University of Genua (http://www.lambs.it)

Figure **18** shows a laboratory set-up for 2PE-MPE microscopy. Figure **19** shows an example of optical sectioning performed through a sphere as compared to conventional confocal optical sectioning, while figure **20** shows 2PE optical slices from a thick sample taken by exploiting the autofluorescence signal. Figure **21** and figure **22** demonstrate the multiple fluorescence imaging capability and the ability to perform single molecule fluorescence imaging and switching, respectively. Once a MPE architecture has been realized, the

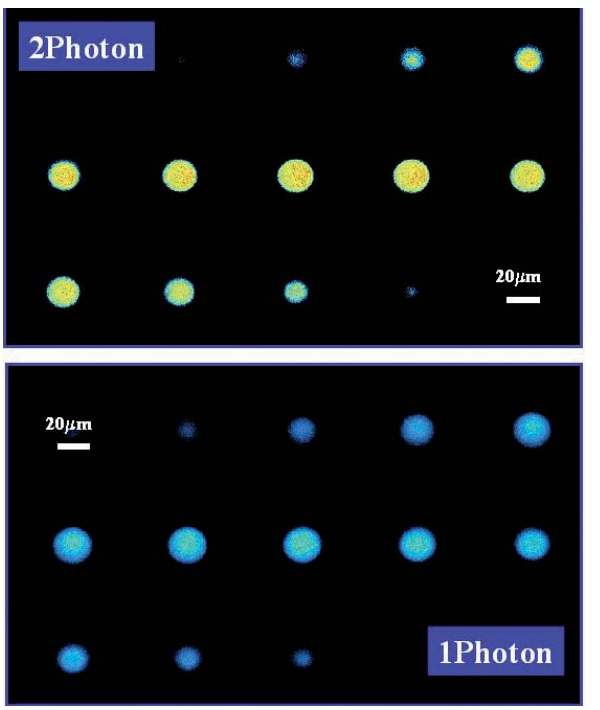

Figure **19**: Example of optical sectioning of fluorescent beads in confocal mode (bottom) and by two photon excitation (top).

following parameters need keeping under control: power and pulse width at the sample focal plane checking for the square intensity/power behaviour, spectral separation of the emitted fluorescence including removal of the possible excitation reflections that could be particularly subtle, z-axis precise control and laser-scanning system alignment.

Recent developments have implemented intense 2PE dedicated laser sources for producing white light laser lines, creating outstanding new application potential for MPE architectures, especially for those featuring precise and fast control of the excitation laser lines.

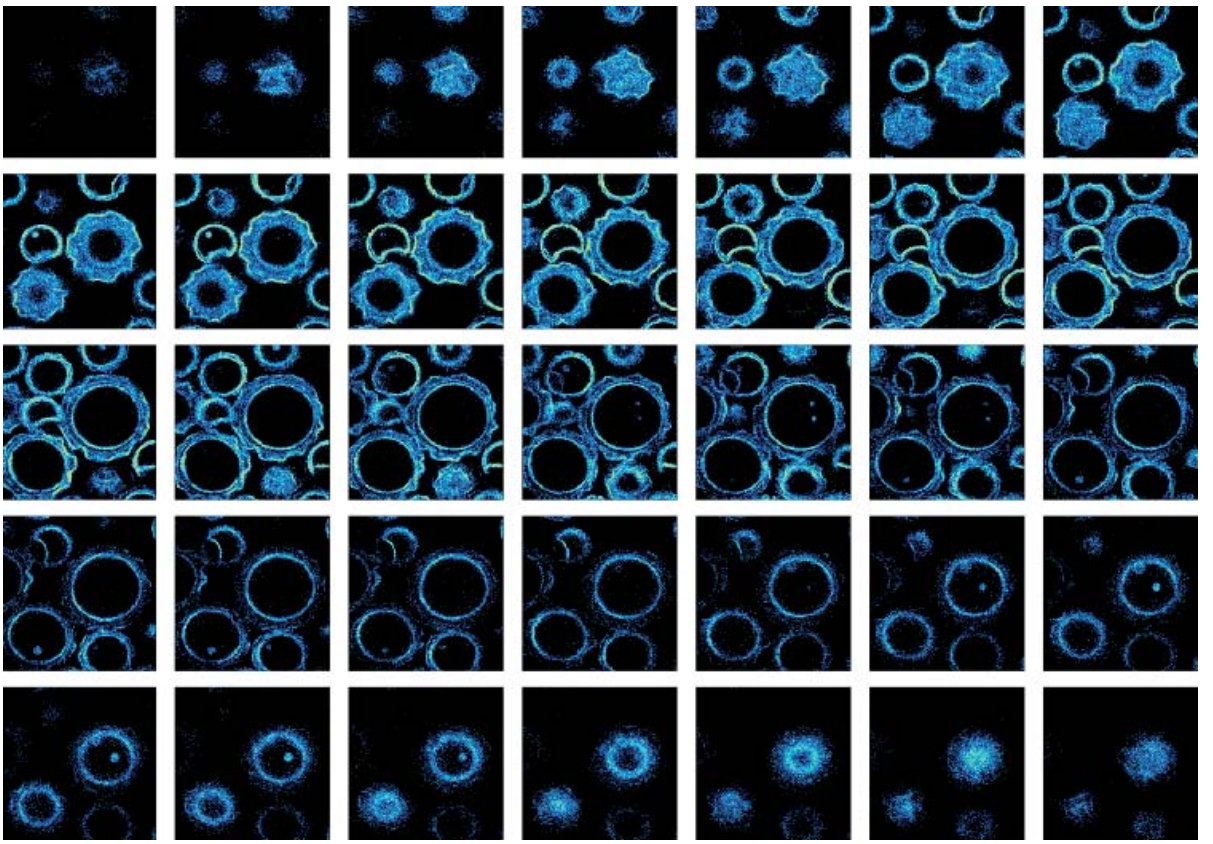

Figure **20**: Example of optical slicing in 3D using the autofluorescence in membranes that form cysts in *Colpoda* (courtesy R. Ramoino, DIPTERIS, University of Genua). The optical sections are taken step by step through the sample.

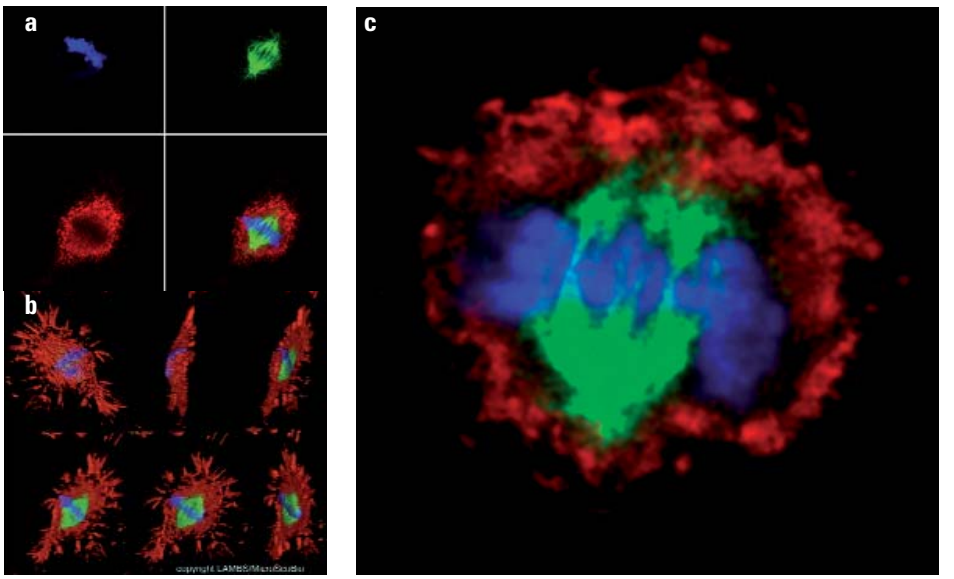

Figure **21 a, b, c**: Example of images obtained by two-photon excitation (740 nm) in multi fluorescence: **a**) view of three channels and the overlay in a single image. **b**) view of the resulting 3D images. **c**) result of a 3D projection. (The images were recorded during the practicals of the Advanced Fluorescence Course by Alberto Diaspro and Gazia Tagliafierro Sample preparation by Laura Girosi and Sara Ferrando. Imaging by Paolo Bianchini).

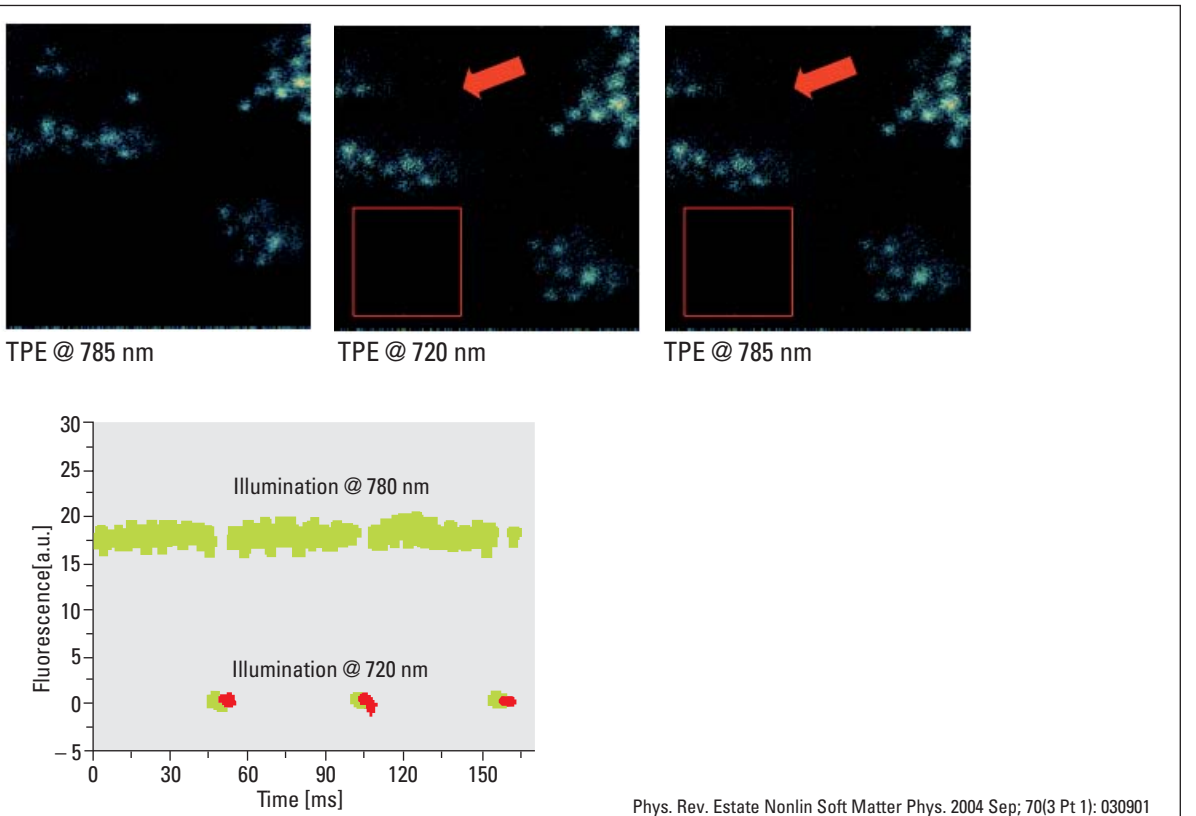

Phys. Rev. Estate Nonlin Soft Matter Phys. 2004 Sep; 70(3 Pt 1): 030901

Figure **22**: Increased signal-to-noise allows imaging of single molecules. In this case, not only the fluorescence signal of a single protein is shown, but also the capacity of molecules to pass states of ON and OFF in terms of fluorescence emission (Project of Alberto Diaspro, Fabio Cannone, Giberto Chirico, Vittorio Pellegrini, Fabio Beltram).

3.5 Open Scenarios and Trends

2PE and MPE microscopes are expected to have an increasing impact on areas such biotechnology, neurobiology, embryology, tissue engineering and materials science, where imaging can be coupled to the possibility of using such microscopes in an active way, too. Clinically, 2PE may find applications in non-invasive optical bioscopy, while in cell biology the imaging abilities are coupled to the possibility of producing highly localized chemical reactions. Potential applications in integrative cardiac physiology or tracking for long time biological events in living systems point out to the ability to make direct observations of phenomena and circumstances that before could only be inferred using different approaches.

The great quantity of new investigation methods offered by 2PE/MPE microscopy enlarges the fields of application in such a way that it is not possible to give a full list of all the possible variations. For this reason, this last paragraph gives a summary of the main properties of MPE and a limited overview of paramount trends. The great impact of 2PE in optical microscopy is related to the fact that it couples a three-dimensional intrinsic ability with five other interesting capabilities, namely: first, 2PE greatly reduces photo-interactions and allows imaging of living specimens over long time periods; second, it allows operation in a high-sensitivity signal-to-noise acquisition scheme; third, 2PE microscopy can penetrate turbid and thick specimens down to a depth of a few

hundreds of micrometers; fourth, due to the distinct character of the multiphoton absorption spectra of many of the fluorophores 2PE allows simultaneous excitation of different fluorescent molecules, reducing colocalization errors; fifth, 2PE can prime photochemical reactions within subfemtoliter volumes inside solutions, cells and tissue. Other points worth mentioning are the design of application suited fluorophores; the development and utilization of so-called quantum dots; the use of visible and photoactivatable fluorescent proteins from the green fluorescent protein (GFP) and its natural homologues to specifically engineered variants or enhanced hybrid molecules, the use of photoswitchable proteins to break the diffraction barrier in fluorescence microscopy at low light intensities.

Furthermore, this form of non-linear microscopy also favored the development and application of several investigation techniques, among them: three-photon excited fluorescence, second harmonic generation, third-harmonic generation, fluorescence correlation spectroscopy, image correlation spectroscopy, single molecule detection; photodynamic therapies, and flow cytometry. A further mention is due to biomolecular tracking in real time and *in vivo*. Here 2PE and MPE can be considered as the dominant technologies. A special application is *in vivo* brain imaging realized by means of a newly designed compact and portable 2PE micro endoscope recently used to visualize hippocampal blood vessels in the brains of live mice.

A first partial view into the dynamics of developmentally programmed, long-range cell migration in the mammalian thymus was also obtained using 2PE in a 4D (x-y-z-t) manner. The movement of thymocytes was recently followed in real time through the cortex within intact thymic lobes. All these facts point to the fact that MPE enables a 7D exploration of living cells to be performed due to its inherent ability in (x-y-z-t) that can be integrated by spectral, lifetime and susceptibility information coming from the samples and complemented by FLIM (Fluorescence Lifetime Imaging Microscopy), FRAP (Fluorescence Recovery After Photobleaching), FRET (Förster-fluorescence Resonance Energy Transfer) and SHG (Second Harmonic Generation) methods. Additionally, regardless of the fact that all far field light microscopes are limited in the achievable diffraction-limited resolution, MPE is pushing modern light microscopy towards fluorescence optical nanoscopy, allowing better exploitation of non linear processes behind the emission of fluorescence from dyes and proteins.

Now, since the technique is still in its infancy and there is a proliferation of new applications and variations on the theme, we think that a good start is made by gaining experience on a good confocal microscopy system, possibly equipped with spectral detection, fast scanning and flexible configuration both for excitation and detection.

4

4. Bibliography

Relevant articles on single and multi-photon confocal microscopy.
More articles by the authors and other relevant references can be found under the following address:
http://www.ncbi.nlm.nih.gov/sites/entrez.

- Amos, W.B., White J.G. (2003) How the Confocal Laser Scanning Microscope entered Biological Research. Biology of the Cell **95** 335–342.
- Arndt-Jovin D.J., Nicoud R.M., Kaufmann J., Jovin T.M. (1985) Fluorescence digital-imaging microscopy in cell biology.'Science, **230**, 13330-1335.
- Bastiaens P.I., Hell S.W. (eds.) (2004) Recent Advances in LightMicroscopy. Journal of Structural Biology. **147**, 1-89. Becker W. (2005) Advanced Time-Correlated Single Photon Counting Techniques. Springer Publ.
- Beltrame, F., Bianco, B., Castellaro, G., Diaspro, A. (1985) Fluorescence, Absorption, Phase-contrast, Holographic and Acoustical Cytometries of Living Cells. in: Interactions between Electromagnetic Fields and Cells. (Chiabrera A.,et al. eds.). NATO ASI Series, vol.97, Plenum Press Publishing, New York and London, 483-498.
- Birks, J.B. (1970). Photophysics of Aromatic Molecules. London: Wiley Interscience.
- Brakenhoff, G.J., van der Voort, H.T.M., van Spronsen, E.A. Linnemans, W.A.M. & Nanninga. (1985) Three-dimensional chromatin distribution in neuroblastoma nuclei shown by confocal scanning laser microscopy. Nature, **317**, 748-749.
- Castleman K.R. (1996). Digital Image Processing. Englewood Cliffs (NJ): Prentice Hall.
- Chalfi e, M., Kain, S. (1998). Green Fluorescent Protein, New York: Wiley Liss.
- Denk, W., Strickler, J.H., Webb, W.W. (1990). Two-photon laser scanning fl uorescence microscopy. Science **248**, 73-76.
- Diaspro A. (ed.) (2001) Confocal and two-photon microscopy: foundations, applications, and advances. Wiley-Liss, New York. Hell SW. (2003) Toward fluorescence nanoscopy. Nat Biotechnol. **21**, 1347-55. 100
- Lakowicz, J.R. (1999). Principles of Fluorescence Microscopy. New York, Plenum Press.
- Masters, B.R. (1996) Selected Papers on Confocal Microscopy. SPIE Milestone series, SPIE Press, Bellingham, WA.
- Masters B.R. (2002) Selected Papers on Multiphoton Excitation Microscopy, SPIE Milestone Series, SPIE Press, Bellingham, WA.
- Matsumoto, B. (Editor) (2002) Cell Biological Applications of Confocal microscopy (2nd ed.), Methods in Cell Biology series, vol.70, Academic Press, San Diego - London.
- Minsky, M. (1988) Memoir of Inventing the Confocal Scanning Microscope. Scanning. **10**, 128-138.
- Pawley, J. B. (ed.). (2006). Handbook of Biological Confocal Microscopy. 3rd edition. New York: Plenum Press.
- Periasamy, A. (ed.) (2001) Methods in Cellular Imaging, Oxford University Press, New York.
- Periasamy A., Day R.N. (2005) Molecular Imaging: FRET Microscopy And Spectroscopy. Oxford University Press, New York.
- Robinson, J.P. (2001). Current Protocols in Cytometry. New York: John Wiley & Sons.
- Sheppard C.J.R., Shotton D.M. (1997) Confocal Laser Scanning Microscopy, BIOS Scientifi c Publ., UK.
- Shotton D.M. (1993). Electronic Light Microscopy. Techniques in Modern Biomedical Microscopy, Vol.1 New York: Wiley-Liss.
- Svelto O. (1998). Principles of Lasers (4th edition) New York: Plenum Press.
- Wilson, T., Sheppard, C.J.R. (1984). Theory and Practice of Scanning Optical Microscopy. London: Academic Press, London.
- Wilson, T. (1990). Confocal Microscopy. London: Academic Press.

Acknowledgements

Watching, observing, and learning. In my work and in my life. My warmest thank-you goes to the people who have watched, observed, and taught me, and who have been present every day with their advice, their love, and their friendship.

A second thank-you obviously goes to those who gave me the work tools needed to watch and try to understand, and to the person who organized this project, for giving me the chance to "broadcast" these minor observations.

Finally, two dedications: To Francesca, to whom I owe the greatest memories of our lives, favorite observer and observed; And to all those people, especially Bruno and Patrizia, who are forced to search within them for the strength to live, when something invisible suddenly breaks inside their bodies.

M. F.

Using a microscope, of any kind, has always been my dream, since I was a kid. I have been lucky to have the opportunity to work with nearly all the microscopy techniques, and for that I am grateful to many people. The optical microscope became my obsession at the University, I was absolutely intrigued by the possibility of using it to observe samples that are not visible. Bruno Bianco, Francesco Beltrame, Alessandro Chiabrera, and Massimo Grattarola, who were pioneers in the emerging bioengineering field in the eighties, provided me with opportunities and taught me how. Francesco Beltrame is still one of the people I am closer in the world of science. Alessandra Gliozzi - who fostered the birth of the multi-photon microscopy field in Italy together with Salvatore Cannistraro - let me bring my passion to the department of physics. Cesare Usai is the enthusiastic scientist I had the pleasure to work with, and I have always been in tune with the adventure of the two photons, since the beginning. Paola Ramoino has always shown patience, as the biologist/microscopist in the group. Carlo Tacchetti allowed me to widen my horizons with his astute and important ideas about cellular traffic and cross-fire in electron microscopy. I am in debt for having met and worked with people like PierPaolo Di Fiore and Piergiuseppe Pelicci, and their groups.

The Two Photon adventure continued and expanded in Genoa, with the help of piles of focaccia bread, with Giberto Chirico, Fabio Cannone, Sabrina Beretta, Maddalena Collini, and Laura D'Alfonso from Giancarlo Baldini's group at the Milano Bicocca University. My partnership with Mario Faretta has been one of my most rewarding experiences in my work on microscopy and in my life. Because of the limited space, I am not able to mention all the people I worked with. But there are many other people that I need to thank. I am going to do it in no particular order, and I apologize in advance to anyone I missed. For several reasons, I am in debt to Cristiana Ricci, Enrico Ambi, and Paolo Sapuppo, who believed and believe in the LAMBS project. I am deeply grateful to Enrico Gratton, who was extremely patient in explaining me the two photons microscopy (among other things), to Giuliano Colombetti and Umberto Fascio for the useful discussions we had, and to several colleagues who have fended a barrage of questions and patiently provided answers.

In no particular order, thanks also to: Massimo Scauso, Fred Brakenhoff, Grazia Tagliafierro, Luciana Dini, David Piston, Peter So, Ammasi Periasamy, Daniel Farkas, Satoshi Kawata, Min Gu, Stefan Hell, Tony Wilson, Colin Sheppard, Petra Schwille, Brad Amos, Barry Masters, Peter Torok, Hans Gerritsen, Martin Hoppe, Rolf Borlinghaus, Irmtraud (Irmi) Steinmetz, Michael Stanley, Marteen Balzar, Jeffrey Larson, Stan Schwartz, Rafael Storz, Matthew Issoukis, Werner Knebel, Alvar Piera, Raniero Centrone, Tanjez Szellas, Volker Seyfried, Jim Mc Nally, Karsten Konig, John Girkin, Franco Conti, Lucia Kubinova, Pino Arcovito, Francesco Pavone, Marc Schneider, Munish Chanana, Fabio Beltram, David Wokosin, Gail McConnell, Christian Soeller, Hans van der Voort, David Dunlap, Laura Finzi, Carlos Bustamante, Carlo Pellicciari, Paola Barboro, Ted Young, Weyming Yu, Beniamino Barbieri, Tiziana Parasassi, Jim Pawley, Beppe Starace, Ranieri Rolandi, Giuliano Mazzini, Franco Gambale, Anna Boccaccio, Vincent Torre, Francesca Bertani, Kees van Oord, and many others.

Apologizing in advance for any omission, I need to mention: The wonderful men and women of LAMBS (in alphabetical order): Paolo Bianchini, Valentina Caorsi, Francesca Cella, Silke Krol, Raffaella Magrassi, Davide Mazza, Federica Morotti, Mattia Pesce, Emiliano Ronzitti, Ilaria Testa, Giuseppe Vicidomini; Grandpa Mario (Arace) for that oscilloscope that I always have with me since 1978;Osamu Nakamura, Miguel Aguilar, Swamy Laxminaraian, Gianfranco Menestrina, and Ivan Krekule, who are not with us anymore and who helped me a lot.

A special thank you to Teresa, Claudia, and Alvina the bunny, for sharing and continuing to share the microscope images with me.

The LAMBS thanks Fondazione San Paolo for their proactive support.
A.D.

Order no. of the edition: English 1593107002 • ??/08/???/???? • LEICA and the Leica Logo are registered trademarks of Leica IR GmbH.